NACA

RESEARCH MEMORANDUM

AN INVESTIGATION OF THE EFFECTS OF JET EXHAUST AND REYNOLDS NUMBER UPON THE FLOW OVER THE VERTICAL STABILIZER AND RUDDER OF THE DOUGLAS D-558-II RESEARCH AIRPLANE AT MACH NUMBERS OF 1.62, 1.93, AND 2.41

By Carl E. Grigsby

Langley Aeronautical Laboratory
Langley Field, Va.

NATIONAL ADVISORY COMMITTEE
FOR AERONAUTICS

WASHINGTON
June 17, 1954

NATIONAL ADVISORY COMMITTEE FOR AERONAUTICS

RESEARCH MEMORANDUM

AN INVESTIGATION OF THE EFFECTS OF JET EXHAUST AND REYNOLDS NUMBER UPON THE FLOW OVER THE VERTICAL STABILIZER AND RUDDER OF THE DOUGLAS D-558-II RESEARCH AIRPLANE AT MACH NUMBERS OF 1.62, 1.93, AND 2.41

By Carl E. Grigsby

SUMMARY

An investigation has been made to determine the effects of jet exhaust and Reynolds number upon the flow over the vertical stabilizer and rudder of the Douglas D-558-II research airplane with special attention to an understanding of the rudder reversals experienced in flight on the full-scale airplane. Tests were made at Mach numbers of 1.62, 1.93, and 2.41 over a range of ratios of jet static pressure to stream static pressure from the jet-off ratio to about 40 and for a maximum range of sideslip angles of $\pm 6^{\circ}$. Four different techniques were used in the investigation: pressure distribution over the vertical tail, free-floating-rudder tests, ink-flow studies, and schlieren photographs. Analysis of the results has shown that, at the lower Mach numbers, an analogy exists between the flow characteristics for the vertical tail (without horizontal tail) and the characteristics for a delta wing having a round leading edge. Rudder reversals were shown to occur at large values of the jet static-pressure ratio as a result of jet interference. The interference effect of varying jet static-pressure ratio was found to be confined to a small range of both angles of sideslip and angles of attack and to decrease with increasing Mach number, becoming insignificant at Mach number of 2.41. The effect of varying both jet pressure ratio and Reynolds number upon the sideslip coefficients and derivatives for the vertical tail was small at the Mach numbers tested.

INTRODUCTION

In a recent flight of the Douglas D-558-II research airplane, measurements of the rudder hinge-moment coefficient were made which differed

greatly for the power-on and the power-off conditions. For example, data from reference 1 show that, at a Mach number of 1.8 and an altitude of 62,000 feet, a value of rudder hinge-moment coefficient of 0.014 was obtained for power-on flight and a value of -0.001 for power-off flight. In addition, flight tests of the X-1 research airplane (ref. 2) have shown that at supersonic speeds, the effect of the jet pressures may be felt forward of the base as much as one base diameter. Both the D-558-II and the X-1 are rocket powered and the rocket installations are similar.

Preliminary results presented in reference 3 have afforded a possible explanation of the mechanism producing rudder reversals. Although the results suffer from having the wake of the support strut in the same plane as the vertical tail, the data indicate that the high jet pressures are felt forward on the low-pressure side of the body and vertical tail and cause the boundary layer to separate. The resulting shock was believed to cause the rudder reversals.

In order to examine in detail the effects of jet pressure upon the flow field over the vertical stabilizer and rudder of the D-558-II research airplane, an investigation has been made in the Langley 9-inch supersonic tunnel of a 1/63-scale model having the essential features of the D-558-II airplane. The rear portion of the flight configuration was duplicated in the model, except that the model did not have a horizontal tail. Tests were made for a cold-jet condition at Mach numbers of 1.62, 1.93, and 2.41 over a range of ratios of jet static pressure to stream static pressure from the jet-off value to about 40 and for a maximum range of sideslip angles of $\pm 6^{\circ}$. Previous experience with jets without secondary flows, based on unpublished data, has shown that at supersonic speeds cold-jet data may be used to predict hot-jet characteristics.

SYMBOLS

b wing span (span of full-scale airplane × scale factor 1/63)

C_Y lateral-force coefficient, $\frac{\text{Lateral force}}{qS}$

C_n yawing-moment coefficient, $\frac{\text{Yawing moment}}{qSb}$

C_l rolling-moment coefficient, $\frac{\text{Rolling moment}}{qSb}$

c local chord of vertical tail

c_N section normal-force coefficient, measured in yaw direction

c_{N_c}	chordwise section-loading coefficient for vertical tail
h	tail height above body center line
M	free-stream Mach number
P	pressure coefficient, $\frac{p_l - p_s}{q}$
p_s	free-stream static pressure
p_l	local static pressure
p_j	jet static pressure at nozzle exit
q	free-stream dynamic pressure
R	free-stream Reynolds number based on model length
S	wing area $\left(\text{area of full-scale airplane} \times \left(\frac{1}{6.3}\right)^2\right)$
x, z	vertical-tail coordinates
α	angle of attack
β	sideslip angle
δ_r	rudder angle; measured from axis of model, positive for clockwise values when viewed from top of model
γ	ratio of specific heat at constant pressure to specific heat at constant volume

Subscripts:

t	refers to vertical tail
β	derivative of sideslip coefficient with respect to sideslip angle

APPARATUS AND TESTS

Tunnel

The Langley 9-inch supersonic tunnel is a continuous-operation, closed-circuit type of wind tunnel in which the pressure, temperature,

and humidity of the enclosed air can be regulated. Different Mach numbers are provided by interchangeable nozzle blocks which form test sections approximately 9 inches square. Eleven fine-mesh turbulence-damping screens are installed in the relatively large-area settling chamber ahead of the supersonic nozzle. A schlieren optical system is provided for qualitative flow observations.

Models

A drawing of the model and supports giving the principal dimensions is shown in figure 1. Although it was desirable that the flight configuration be duplicated, a number of modifications were necessary. These modifications were, in general, of a minor nature, and it is believed that they would contribute no significant effect upon the results of this investigation. The leading-edge-sweep angle of the wing was maintained although the wing did not taper in chord or in thickness as did that of the full-scale airplane. The slight modifications to the wing section and to the vertical tail section which were necessary to give more thickness near the trailing edge are shown in figure 1. As can be seen in figure 1, the test model did not have a canopy or the horizontal tail. With the pressure tubes imbedded in the surface of the vertical tail, it was impossible to support the horizontal tail. Also, because of an error in machining, the area ratio of the exhaust nozzles was not duplicated. Calibration of the nozzles indicated the exit Mach number to be 2.0 ± 0.1; whereas the Mach number of the full-scale rockets is 2.7 (as determined on the basis of the area ratio and with γ assumed to be 1.4). Unpublished results have shown that differences in Mach number of this order have only small effect upon base pressure in this range of jet Mach numbers.

The simulated wing served as a support for the model, so that variations in angle of sideslip were permitted with the tunnel operating. The left wing panel served as a duct for the high-pressure jet air. The right wing panel served as a conduit for the pressure tubes mounted in the vertical fin. A settling chamber of relatively large area was provided inside the body immediately ahead of the removable nozzle section, which is shown in detail in figure 1.

The vertical stabilizer and rudder is shown in figure 2. Because of the small size of the model, only ten pressure tubes could be installed in the vertical tail, and the following procedure was established to obtain the different orifice locations. Tests at each Mach number covering the complete range of test variables were made for a given set of ten orifice locations. These orifices were filled and new locations drilled. The complete sequence at each Mach number was then repeated. The maximum deviation of the vertical-tail plan form of the tunnel model from the scaled-down plan form of the flight airplane (as shown in figure 2) was about 0.020 inch.

Photographs illustrating the tunnel setup are shown in figure 3(a). The angle-of-sideslip mechanism is shown in the upper photograph. The sideslip-angle range was limited to those angles free of interference from the support struts. This angle range was established at each Mach number by schlieren observation, and by visual observation of the changes in the pressures over the vertical tail as sideslip angle was varied. Details of the two floating rudders tested are shown in figure 3(b), and the rudder outline is shown in figure 2. The basic rudder has the same section as the trailing-edge section of the vertical tail, whereas the slab rudder had constant-thickness sections having the same thickness as the basic rudder at the hinge line. The rudders were supported on small pins which gave small resistance to rotational movement.

Tests

The tests were divided into four categories:

(a) Measurements of the pressure distribution over the vertical stabilizer and rudder.

(b) Ink-flow studies of the flow field over the vertical tail. Ink was bled from the two orifices indicated on figure 2.

(c) Free-floating rudder tests.

(d) Schlieren photographs of the model in both horizontal and vertical position.

The model was mounted as shown in figure 3(a) for all tests except those in which schlieren photographs were made of the model in a vertical position. The rudder angles in the free-floating rudder tests were measured by reflecting a light beam from a small mirror imbedded in the rudder onto a calibrated scale. The free-floating rudders were not mass balanced; an attempt to balance the basic rudder with the use of bob-weights was unsuccessful because of the high drag of the balance weights. Early attempts to obtain results with the basic rudder were unsuccessful as a result of rudder oscillations; the slab rudder was tested in an attempt to reduce these oscillations by changing the natural frequency of the rudder.

Tests were made with the transition fixed by a transition strip of crushed salt particles extending from the leading edge of the vertical tail to about the location of the first orifice at each station. The extent of the transition strip is indicated on figure 2. The tests with the transition strip were made to duplicate high Reynolds number conditions while maintaining the large jet pressure ratios, since it was impossible to obtain high Reynolds numbers and large jet static-pressure ratios simultaneously.

A comparison of flight and tunnel test conditions together with the range of tunnel test variables is given in the following tables:

Flight			
M	Altitude, ft	p_j/p_s	R
1.62	60,000	9.6	46.12×10^6
1.62	80,000	25.0	19.21
1.93	60,000	9.6	59.50
1.93	80,000	25.0	22.90

Tunnel				
M	p_j/p_s	α	β	R
1.62	Off to 37.57	0°, 5°	2°	0.95×10^6
1.62	Off	0°, 5°	2°	8.14
1.93	Off to 39.32	0°, 5°	4°	1.30
1.93	Off	0°, 5°	4°	7.28
2.41	Off to 41.66	0°, 5°	6°	2.05
2.41	Off	0°, 5°	6°	5.96

PRECISION OF DATA

The model was located within ±0.10° of zero pitch and zero sideslip with respect to the tunnel center line and tunnel sidewalls, respectively. Previous measurements of the flow angularity in the test section have shown negligible deviations. The pressure coefficients have not been corrected for any variation in stream static pressure. The estimated accuracies of the test variables and coefficients are given in the following table:

Mach number, M	±0.01
Reynolds number, R	$\pm 0.03 \times 10^6$
Pressure coefficient, P	±0.002
Angle of attack, α	±0.05°
Angle of sideslip, β	±0.10°
Rudder angle (relative)	±0.02°
Rudder angle (initial)	±0.25°

RESULTS

The figures will be presented and their contents described briefly before discussion of the results, since it is believed that a more thorough understanding of the results may be obtained by a simultaneous discussion of related figures. The discussion of the results is concerned principally with the effects upon the characteristics of the vertical tail of variations in the main parameters of the investigation - that is, jet static-pressure ratio, angle of sideslip, Reynolds number, angle of attack, and Mach number.

The pressure distributions over the vertical stabilizer and rudder at $M = 2.41$ for various sideslip angles and jet static-pressure ratios are shown in figure 4. The corresponding pressure distributions at $M = 1.93$ are shown in figure 5 and at $M = 1.62$, in figure 6. Only the pressure distributions at $\alpha = 0^\circ$ are shown although results were obtained at both 0° and 5° angle of attack. Curves are faired through the results for the low Reynolds number jet-off condition, for the maximum jet static-pressure-ratio data, and for the high Reynolds number jet-off condition.

Typical curves illustrating the effect of varying angle of attack upon the pressure distribution over the vertical stabilizer and rudder for $M = 1.93$ with the jet off are shown in figure 7.

An attempt was made to duplicate high Reynolds number conditions over the rudder by fixing transition with a transition strip along the leading edge of the vertical tail. Typical pressure distributions illustrating the effect of fixing transition for a jet-off condition are shown in figure 8 for vertical station $2\left(\frac{z}{h} = 0.643\right)$.

Sketches from results of ink-flow studies of the flow over the vertical tail are shown in figures 9 and 10. These sketches were made from individual frames of motion pictures taken for each sequence of test variables. The effect of variation in Reynolds number, sideslip angle, and angle of attack for the jet-off condition at $M = 1.93$ and 1.62 are shown in figure 9. The effect of varying jet static-pressure ratio at $M = 1.93$ and 1.62 are shown in figure 10. The direction of flow of the ink does not correspond to the flow streamlines outside the boundary layer, but rather is an indication of the direction of pressure gradient. Thus, the direction of flow shown by the arrows on the sketches indicates negative or falling pressure gradients.

The results of the floating-rudder tests for both the basic and slab rudders for $M = 1.62$ are shown in figure 11. Similar tests were made at $M = 1.93$ for the basic rudder with and without balance weights, and for the slab rudder. At this Mach number, however, considerable difficulty was experienced with rudder oscillations and the data are not presented.

Typical schlieren photographs illustrating the effects of variations in jet static-pressure ratio upon the flow over the rear of the model for M = 1.93 are shown in figure 12. Photographs at two stream Reynolds numbers are presented.

The spanwise variation of the integrated section loading coefficients of the vertical tail are given in figure 13 for all Mach numbers. The results cover the complete range of test variables and curves are faired for the low Reynolds number data for the jet-off condition, for the maximum jet pressure ratio, and for the high Reynolds number jet-off condition. The variation of the sideslip coefficients with sideslip angle is shown for all Mach numbers in figure 14. A comparison of the low Reynolds number results with the high Reynolds number results is also made. The variation of the sideslip derivatives for the vertical tail with Mach number is shown in figure 15. Also given is a compilation of wind-tunnel results (refs. 4 and 5) over the Mach number range together with the theoretical results for the complete airplane (ref. 4). In figure 16 the variation of the static-directional-stability derivative with Mach number is presented, and a comparison of wind-tunnel results and flight results is made. The present results were obtained by adding -0.0036 (the value of the derivative for the body-wing configuration from ref. 5) to the values of $\left(C_{n_\beta}\right)_t$ from figure 15.

DISCUSSION

Effect of Varying Jet Static-Pressure Ratio

It was possible to have only a small number of pressure orifices in the rudder area and these were placed near the hinge line. (See fig. 2.) Thus, it was necessary to extrapolate the results to the stabilizer and rudder trailing edge, so that it was difficult to obtain any accurate picture of the rudder reversals from the pressure distributions. Indication of rudder reversal may be seen on the distributions at M = 1.62 (fig. 6). Essentially no effect of variations in jet pressure ratio was found from the pressure distributions at M = 2.41 (fig. 4) and M = 1.93 (fig. 5). An attempt was made to determine the rudder-locked hinge-moment coefficients by integration of the pressures over the rudder area. This integration was made at M = 1.62 for $\alpha = 0^\circ$ and $\beta = \pm 2^\circ$ with the following results:

p_j/p_s	Rudder hinge-moment coefficient
Jet off	0.003
7.55	.004
15.68	.014
23.99	.014
32.48	.020
37.57	.015

These values of rudder hinge-moment coefficient can at best be considered approximate in view of the small forces considered and the necessary extrapolations in the pressure distributions. However, the coefficients do agree as to order of magnitude with the values measured in flight (ref. 1). Similar calculations made for $\alpha = 5^\circ$ gave little systematic variation of hinge moment with jet static-pressure ratio. Examination of the pressure distributions does reveal that the stick-fixed hinge moment of the rudder will be low and only small changes in pressure over the rudder area are necessary to produce large-percentage changes in rudder hinge moment. The effect of variations in jet static-pressure ratio upon the integrated spanwise loadings of the vertical tail (fig. 13) and upon the sideslip coefficients and derivatives was small.

The effect of the jet upon the flow characteristics over the vertical tail (without horizontal tail) as determined from the ink-flow studies at $M = 1.62$ and 1.93 (fig. 10) may be briefly summarized as follows:

1. High-pressure surface: At $\beta = -2^\circ$ for both Mach numbers, the high jet pressures moved forward into the separated region on the vertical tail, the separation point moving forward with increasing jet pressure ratio. The separated region is shown in the pressure distributions to be greatly influenced by changes in Reynolds number; thus, it is probable that the full-scale airplane having considerably higher Reynolds number would not experience this effect. It should also be pointed out that presence of the ink on the tail can alter to some degree the boundary-layer flow over the tail. Thus the location of separation may be in error, but qualitatively the trends are correct. For the condition of $\beta = -4^\circ$, $M = 1.93$, the jet has little effect on the flow over the vertical tail.

2. Low-pressure surface: For all sideslip angles, increasing jet pressure ratio caused the ink flow in the vicinity of the body and the vertical-tail trailing edge to move away from the body and toward the tip. Since the flow follows the direction of decreasing pressure, the results indicate a high pressure area over the lower portion of the rudder which increases with increasing jet pressure. This result

indicates that the mechanism of rudder reversal given in reference 3 is probably present on this configuration. The change in flow direction is greatest at $M = 1.62$ indicating that the high pressure bleed-forward is greatest for this Mach number.

A more direct indication of the effect of the jet upon the rudder characteristics may be seen from the results of the free-floating-rudder tests (fig. 11). Although these results are not directly comparable to the rudder hinge-moment parameter measured in flight, the data give an indication of the stick-free rudder hinge moment. Slight asymmetries in the floating rudder cause the difference between the results for the positive and the negative sideslip angles and may cause the jet-off rudder angle to be slightly in error. Only the variation in rudder angles is important in this case, however. Tests were made at both $M = 1.62$ and $M = 1.93$ but rudder oscillations and flutter at $M = 1.93$ made it impossible to obtain accurate results and consequently the results are not shown. It was possible, however, to obtain some trends in the variation of rudder angles with jet pressure ratio. At $M = 1.62$ the rudder floats at a negative rudder angle. For both rudder configurations at $\alpha = 0^\circ$ and $\beta = \pm 2^\circ$, increasing jet pressure ratio caused the rudder to move into the flow which would correspond to an overbalance condition. The variation of rudder angle with jet pressure ratio was largest for the basic rudder in the turbulent boundary layer (transition fixed) being about 3° at the maximum pressure ratio. At $M = 1.93$ the rudder floats at a positive rudder angle (data not shown). For $\alpha = 0^\circ$ and $\beta = \pm 2^\circ$ only, the variation of rudder angle with jet pressure ratio was smaller at $M = 1.93$ than at $M = 1.62$. At both Mach numbers the jet had little effect upon the rudder when the model was at 5° angle of attack. Also, little jet interference effect was shown at $\beta = \pm 4^\circ$ for both angles of attack at $M = 1.93$. These results thus indicate that the interference effect of the jet was confined to a small angle range for both sideslip and angle of attack.

It was hoped that some further insight into the physical phenomena associated with rudder reversal might be found from schlieren photographs such as are shown in figure 12. It was found, however, that the body and jet flow masked the flow over the vertical stabilizer and rudder to such an extent as to make a detailed analysis impossible. It is apparent that any forward movement of the shock at the jet exit is confined to the region of the juncture of the body and vertical tail, since the exit shock wave can be seen clearly in both views except in that region (see the side view, fig. 12), and the shock is shown to be attached to the model base. It thus appears reasonable to conclude that the mechanism of jet interaction given in reference 3 is generally satisfactory in explaining the present results; however, the interaction is confined to the region of the juncture of the body and vertical tail.

Effect of Varying Sideslip Angle

A discussion of the effects of sideslip angle upon the pressure distribution over the vertical tail can possibly be presented more effectively under the section discussing Reynolds number effects. Some general statements, however, can be made. At Mach number 2.41 (fig. 4), the distributions are of the type expected for this airfoil section with extensive regions of separation shown especially near the tip. The separated regions at the tip increase as the Mach number is decreased to 1.93, probably as a result of the decrease in Reynolds number. A high pressure peak is shown for the results at $R = 1.30 \times 10^6$ and $\beta = -4^\circ$. This pressure peak disappears as the Reynolds number is increased to 7.29×10^6. Little effect of sideslip angle could be determined at $M = 1.62$ since the range was severely limited.

The section loadings shown in figure 13 are of the type to be expected for this type of configuration with peak loading coefficients at $z/h = 0.354$. These peak coefficients are a result of both the geometry of the vertical tail and body-tail interference. The station closest to the body ($z/h = 0.251$) is in the separated flow over the rear of the body, which causes the low and even negative section loading coefficients.

The variation of the sideslip coefficients with sideslip angle (fig. 14) is nearly linear at $M = 2.41$ with some nonlinearities shown at $M = 1.93$. The agreement as to order of magnitude of the sideslip derivatives of the present investigation and the results of reference 5 (fig. 15) is considered satisfactory in view of the differences between the two test configurations. The configuration used in this investigation did not have a horizontal tail and the forces on the body due to the tail were not measured; whereas the configuration of reference 5 had a slightly smaller vertical tail. The difference in the trends with Mach number between the results of the two tests is not understood. This difference in trends is further illustrated in figure 16. A conservative estimate of C_{n_β} of the body due to the tail (approximately 0.0005 at $M = 1.62$) as obtained from reference 6 brings the present results closer in line with the data from reference 5. (The upper value of C_{n_β} at $M = 1.61$ (ref. 5) is measured over a yaw angle range of $\pm 4^\circ$ while the lower value is for $\beta = 0^\circ$). There is some doubt, however, as to the correct variation of C_{n_β} with Mach number for the D-558-II.

The ink-flow patterns given in figure 9 illustrate a number of the effects of varying sideslip angle discussed previously under the pressure distributions. The results at $M = 1.93$ (fig. 9(a)) will be considered first. The extensive regions of separation near the trailing edge are shown for the high-pressure surface at $\beta = -2^\circ$. The

low-pressure surfaces at both $\beta = -2^\circ$ and -4° show separated regions near the tip at low Reynolds numbers. On the high-pressure surface at $\beta = -4^\circ$ a large concentration of ink is shown in the region of the severe high pressure peak. The results at $M = 1.62$ (fig. 9(b)) show clearly a similarity to the flow characteristics of the delta wing reported in the investigation of Hatch and Gallagher (see, for example, fig. 12 of ref. 7). On the low-pressure surface, the ink flows up toward the region of leading-edge separation. The ink flows along the separated region until the ink piles up to such an extent that it flows back toward the trailing edge. This type of distribution is shown for both Reynolds numbers. The large concentration of ink near the release orifice for the high-pressure surface for $R = 0.95 \times 10^6$ is probably associated with the large adverse pressure gradient in that region.

Effect of Varying Reynolds Number

An attempt was made to duplicate high Reynolds number conditions (by the use of transition on the leading edge of the vertical tail) while maintaining the large values of jet static-pressure ratio. This attempt was only partially successful as the flow tended, especially near the tip, to separate at the transition strip and reattach farther downstream as a laminar boundary layer. Typical results of the transition-fixed data are shown in figure 8 where at $M = 2.41$ and 1.93 separation was delayed by the use of the transition strip. At $M = 1.62$, however, the use of transition was unsuccessful in producing high Reynolds number conditions. Thus, the discussion of Reynolds number effects will be confined to a study of flow characteristics over the vertical stabilizer and undeflected rudder with no jet flow.

The effect of varying Reynolds number upon the pressure distribution over the vertical stabilizer and rudder may be summarized as follows. At $M = 2.41$ (fig. 4) the principal effect of increasing Reynolds number was to prevent or delay separation on the low-pressure surface at stations 1, 2, and 3. At stations 4 and 5 the displacement of the pressure-distribution curves for the two Reynolds numbers is believed to be a result of the change in flow direction about the rear of the body as a result of the change in separation on the body with changing Reynolds number. Increasing Reynolds number at $M = 1.93$ (fig. 5) also delayed or prevented separation on the low-pressure surface at stations 1 and 2. The severe high pressure peak on the high pressure at stations 1, 2, and 3 was completely removed as the Reynolds number was increased from 1.30 to 7.29×10^6. Similar effects of increasing Reynolds number as were discussed at $M = 2.41$ are indicated at stations 4 and 5. Large changes in pressure distribution with increasing Reynolds number are shown at $M = 1.62$ (fig. 6). A high pressure peak occurs on the low-pressure surface at stations 1 through 4

for a Reynolds number of 8.14×10^6. Similar high pressure peaks are indicated on the high-pressure surface at stations 3 and 4. The pressure distributions for $R = 8.14 \times 10^6$ compare very well in general shape to the chordwise distributions obtained from table III of reference 7 for a delta wing having 68.4° leading-edge sweep. The Reynolds number of these results was 2.2×10^6 and the corresponding Reynolds number for the present results, based on the mean aerodynamic chord of the vertical tail, is 1.67×10^6. The analogy between the flow of the vertical tail of the D-558-II model without a horizontal tail and a delta wing having round leading edge is evident. Some evidence of the shock waves lying on the vertical tail may be seen at the tail tip in the schlieren photographs of figure 12.

Only random effects of varying Reynolds number upon the spanwise variation of section loading coefficient (fig. 13) are shown at either Mach number with the largest effects occurring at the lower Mach numbers. The effect of increasing Reynolds number upon the sideslip derivatives was to increase the derivatives (fig. 15) with the largest increase shown at the lower Mach numbers.

The ink-flow patterns shown in figure 9 provide an excellent correlation with the Reynolds number effect discussed under pressure distributions. The action of increasing Reynolds number to prevent or delay separation and the removal of the high pressure peak at $\beta = -4°$ are illustrated in figure 9(a). The patterns given for $M = 1.62$ (fig. 9(b)) show that an increase in Reynolds number does not smooth out the flow characteristics as was true for $M = 1.93$. For $\alpha = 0°$ and $M = 1.62$ the ink tends to flow more toward the leading edge as a result of the more negative pressures in that region at the higher Reynolds number. (See fig. 6.) At $\alpha = 5°$, indications of turbulent spreading of the ink are shown at the higher Reynolds number.

Effect of Varying Angle of Attack

Some effect of angle of attack upon the pressure distribution over the vertical tail can be seen from figure 7 for $M = 1.93$. As might be expected the general shape of the curves is unchanged although the separation point and the location of the high pressure peaks are moved forward at the higher angles of attack. Similar results are shown from the ink-flow patterns given in figure 9(a). Some change in the spanwise variation of section loading coefficients (fig. 13) is shown for varying angle of attack. This variation shows up principally as a decrease in the sideslip derivatives at $M = 1.62$ and 1.93 (fig. 15). No effect of varying angle of attack is shown at $M = 2.41$.

CONCLUDING REMARKS

An investigation has been made to determine the effects of jet exhaust and Reynolds number upon the flow over the vertical stabilizer and rudder of the Douglas D-558-II research airplane with special attention given to the understanding of the rudder reversals experienced in flight on the full-scale airplane. Four different techniques were used in the investigation: pressure distribution over the vertical tail, free-floating rudder tests, ink-flow studies, and schlieren photographs. Tests were made at Mach numbers of 1.62, 1.93, and 2.41 over a range of jet static-pressure ratios from jet off to about 40 and for a maximum range of sideslip angles of $\pm 6^{\circ}$. The pertinent results of this investigation are summarized as follows:

Pressure distributions obtained over the vertical stabilizer and rudder have indicated a large effect of Reynolds number, especially at a Mach number of 1.62. Although the detailed pressure distributions at the lower Reynolds number are not comparable to flight results, indication of rudder reversals at the higher jet static-pressure ratios are present. Examination of the pressure distributions, and results of ink-flow studies have shown the flow characteristics over the vertical stabilizer and rudder at the lower Mach numbers to be analogous to that for a delta wing having a round leading edge.

The detailed mechanism of rudder reversal was not conclusively proved; however, it was indicated that the physical model given in NACA RM L52L02a was satisfactory with the jet interference confined to the region of the juncture of the body and vertical tail. Free-floating rudder angles obtained for both the slab rudder and the basic rudder configurations gave rudder reversals for the jet-on condition at a Mach number of 1.62. The rudder angle became more negative with increasing jet static-pressure ratio with a maximum variation obtained for the basic rudder with turbulent boundary layer (fixed transition).

The interference effect of varying jet static-pressure ratio was found to be confined to a small angle-of-sideslip and angle-of-attack range. The interference effect also decreased with increasing Mach number, becoming insignificant at a Mach number of 2.41. The effect of varying either jet static-pressure ratio or Reynolds number upon the sideslip coefficients and derivatives for the vertical tail was small at the Mach numbers tested. Comparison of the sideslip derivatives for the vertical tail with results from another source has shown

differences between the trends with Mach number; consequently, there is some doubt as to the correct variation of the static-directional stability derivative with Mach number.

Langley Aeronautical Laboratory,
National Advisory Committee for Aeronautics,
Langley Field, Va., April 16, 1954.

REFERENCES

1. Ankenbruck, H. O., and Dahlen, T. E.: Some Measurements of Flying Qualities of a Douglas D-558-II Research Airplane During Flights to Supersonic Speeds. NACA RM L53A06, 1953.

2. Knapp, R. J., and Johnson, W. E.: Flight Measurements of Pressures on Base and Rear Part of Fuselage of the Bell X-1 Research Airplane at Transonic Speeds, Including Power Effects. NACA RM L52L01, 1953.

3. Hatch, J. E., Jr., and Savelle, W. M.: Some Effects of a Sonic Jet Exhaust on the Loading Over a Yawed Fin at a Mach Number of 3.03. NACA RM L52L02a, 1953.

4. Queijo, M. J., and Goodman, A.: Calculations of the Dynamic Lateral Stability Characteristics of the Douglas D-558-II Airplane in High-Speed Flight for Various Wing Loadings and Altitudes. NACA RM L50H16a, 1950.

5. Grant, F. C., and Robinson, R. B.: Static Lateral Stability Characteristics of a 1/16-Scale Model of the Douglas D-558-II Research Airplane at Mach Numbers of 1.61 and 2.01. NACA RM L53I29a, 1953.

6. Nielsen, J. N., Kaattari, G. E., and Anastasio, R. F.: A Method for Calculating the Lift and Center of Pressure of Wing-Body-Tail Combinations at Subsonic, Transonic, and Supersonic Speeds. NACA RM A53G08, 1953.

7. Hatch, John E., Jr., and Gallagher, J. J.: Aerodynamic Characteristics of a 68.4° Delta Wing at Mach Numbers of 1.6 and 1.9 Over a Wide Reynolds Number Range. NACA RM L53I08, 1953.

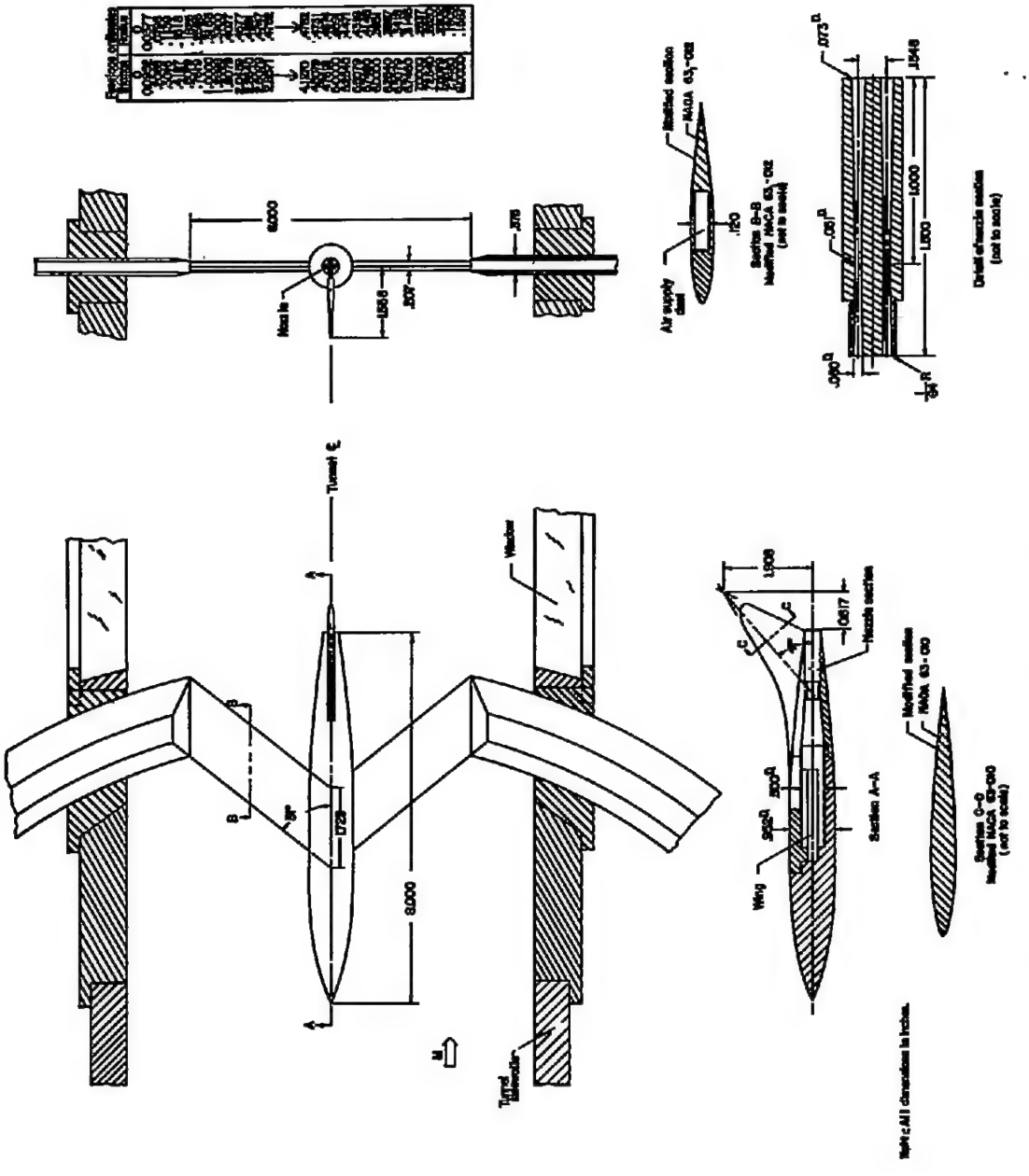

Figure 1.- Drawing of model showing principal dimensions.

Location of Pressure Orifices

Orifice Station Number									
1		2		3		4		5	
z_1, in.	s_1, in.	z_2, in.	s_2, in.	z_3, in.	s_3, in.	z_4, in.	s_4, in.	z_5, in.	s_5, in.
0.245	1.223	0.595	0.996	1.004	0.744	1.314	0.532	0.555	0.329
.144	1.227	.491	.989	.858	.736	1.142	.537	.296	.350
.063	1.228	.386	.982	.713	.728	.960	.546	.271	.344
- .047	1.229	.264	.974	.513	.752	.759	.534	.192	.348
- .118	1.234	.161	.974	.392	.745	.608	.540		
- .217	1.225	.102	.974	.287	.732	.559	.538		
- .275	1.220	- .013	.975	.115	.742	.436	.545		
		- .065	.971	.055	.733				
		- .138	.970	- .029	.741				
s_{ave} = 1.227 in.		s_{ave} = 0.978 in.		s_{ave} = 0.740 in.		s_{ave} = 0.538 in.		s_{ave} = 0.348 in.	

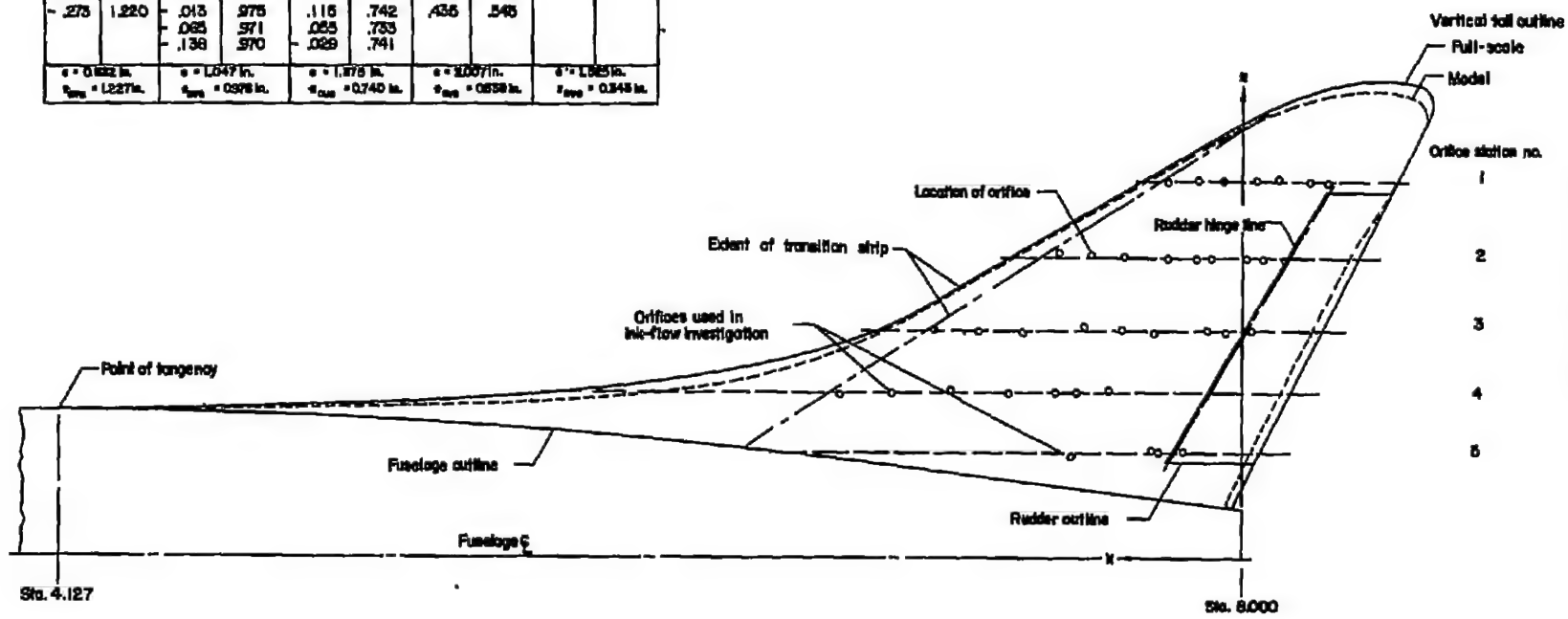

Figure 2.- Details of vertical tail showing locations of pressure orifices.

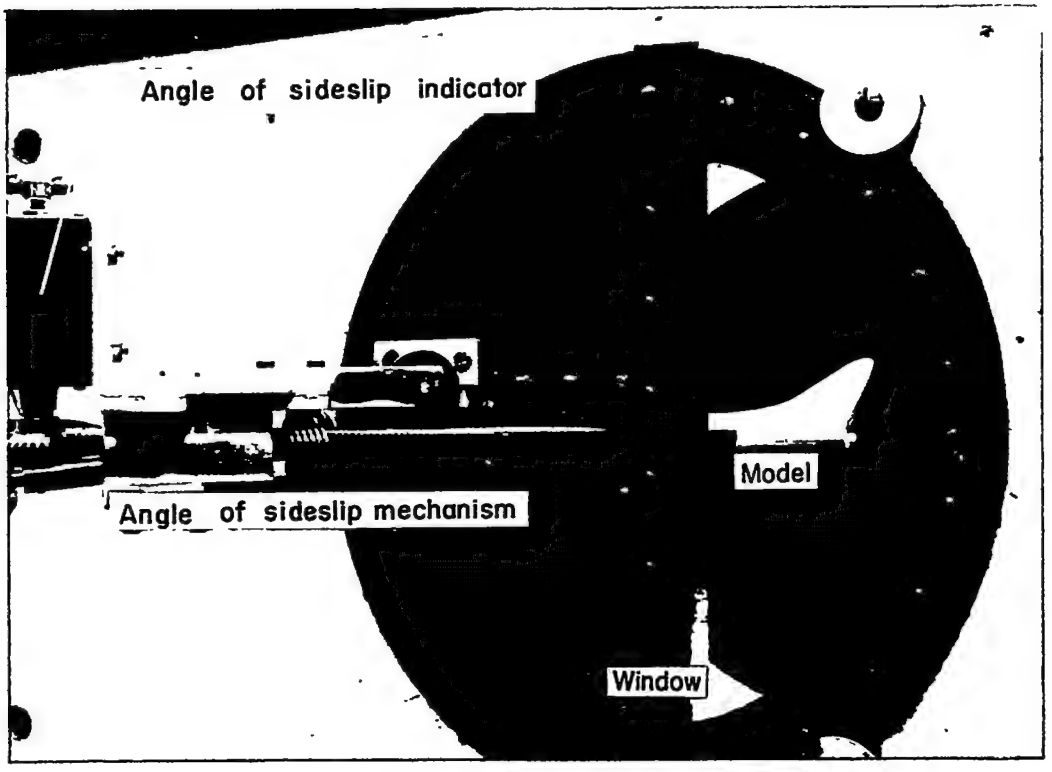

Three-quarter rear view

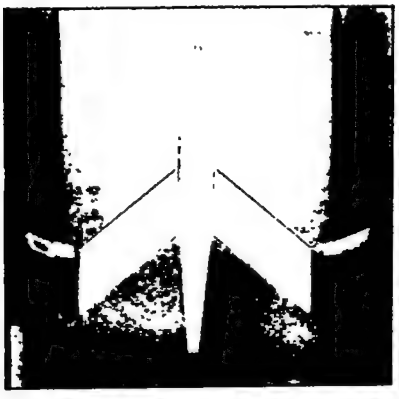

Bottom view

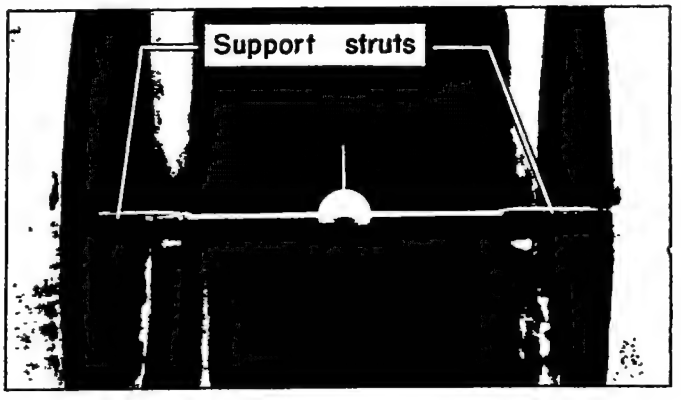

Front view

L-83665

(a) Tunnel setup for pressure distributions, ink-flow studies, and floating-rudder tests.

Figure 3.- Photographs of test setup.

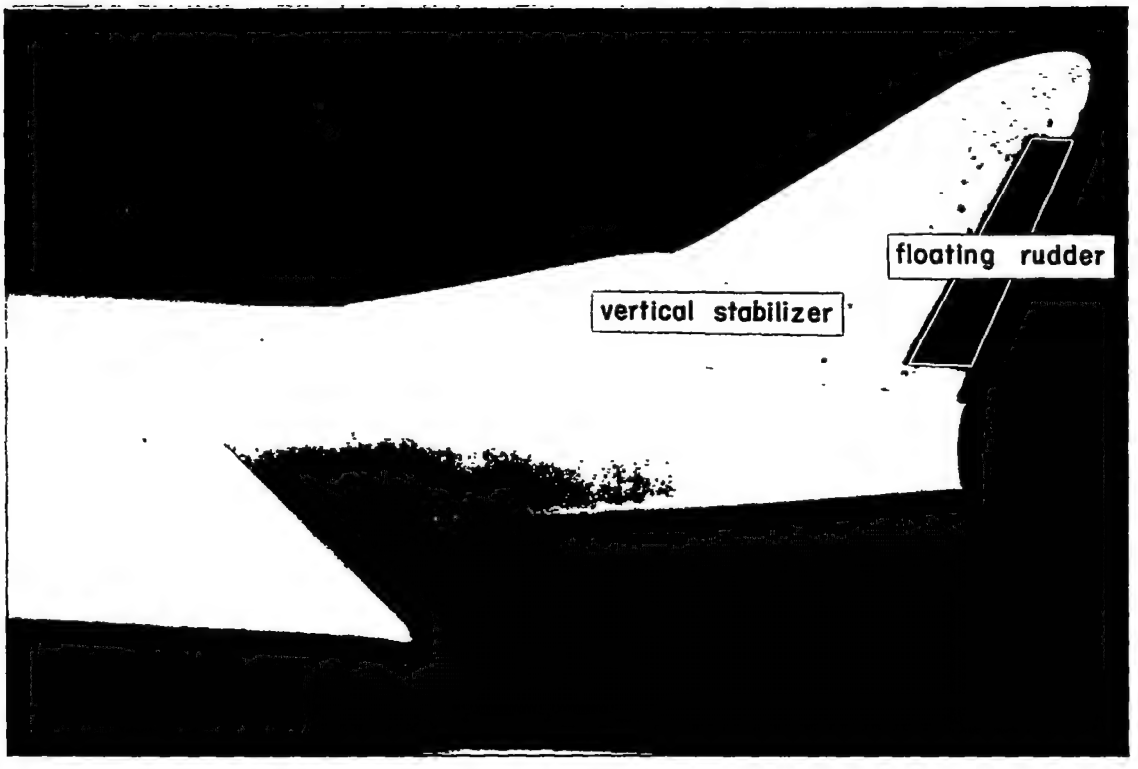

Basic rudder installation

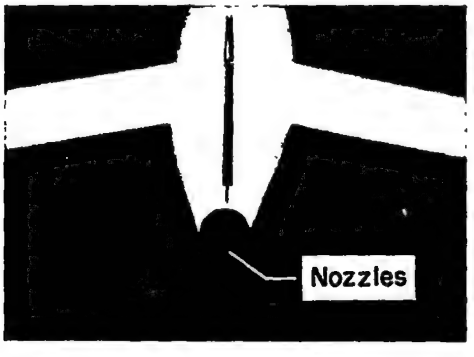

Rear view of slab rudder showing thick trailing edge

L-83666

(b) Floating-rudder installations.

Figure 3.- Concluded.

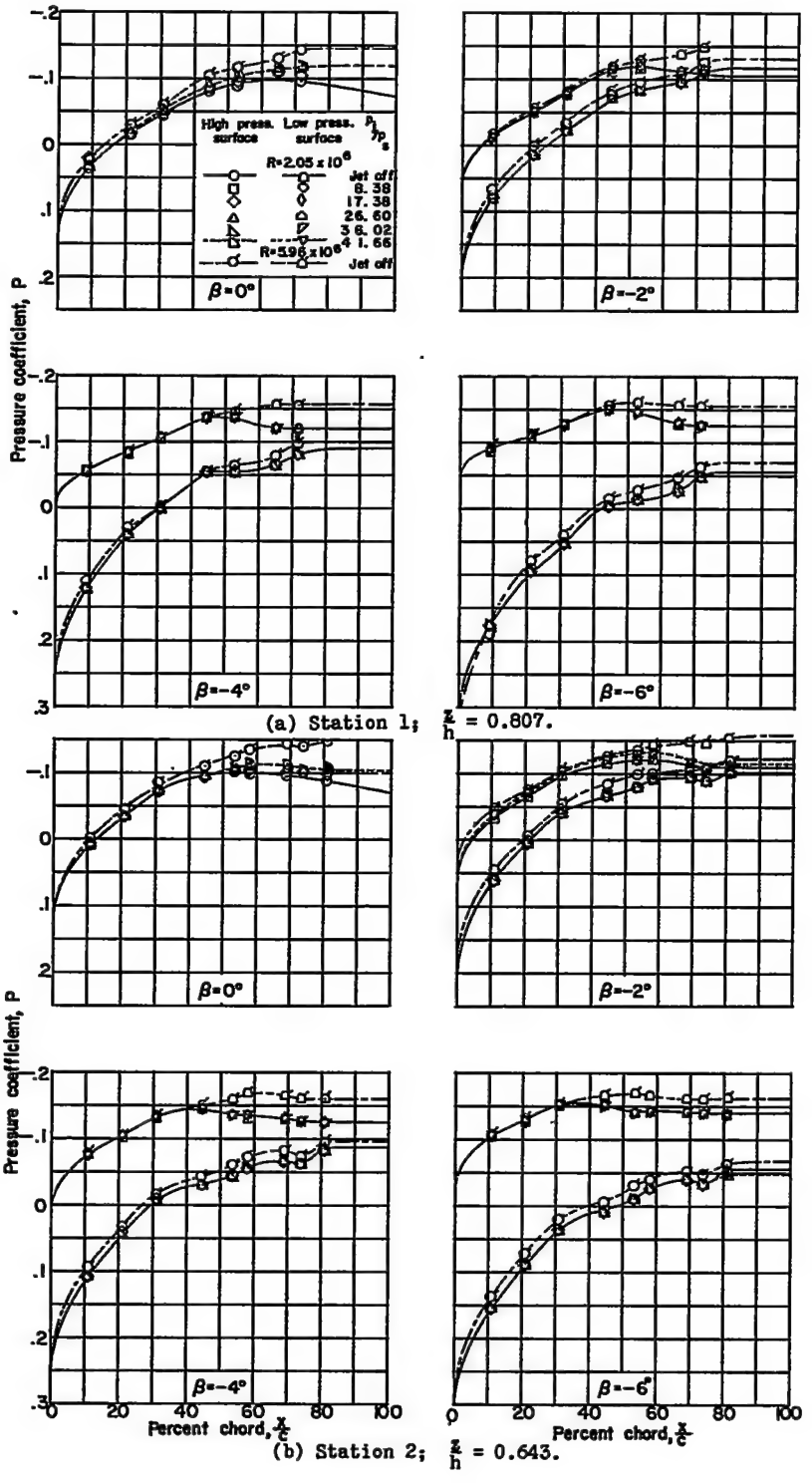

Figure 4.- Effect of varying sideslip angle and jet pressure ratio on the pressure distribution over the vertical stabilizer and rudder at M = 2.41. $\alpha = 0^\circ$; $\delta_r = 0^\circ$.

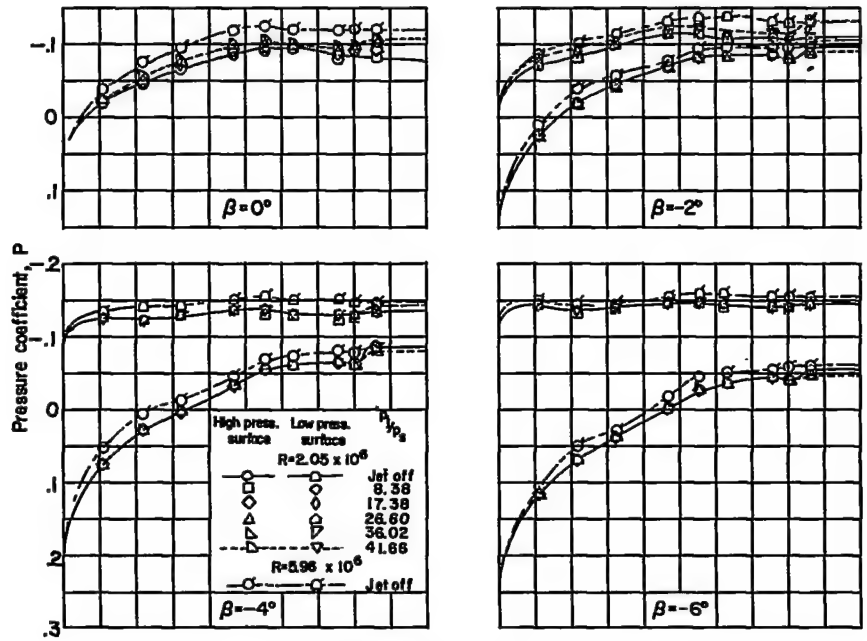

(c) Station 3; $\frac{z}{h} = 0.487$.

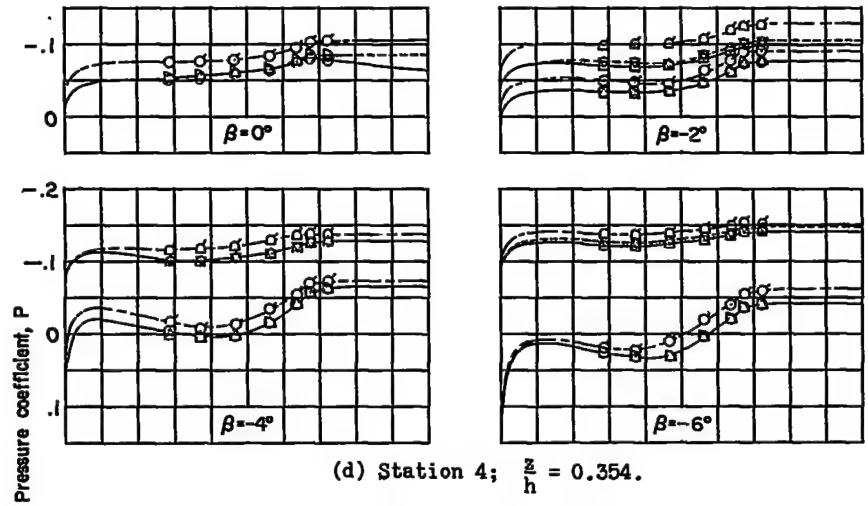

(d) Station 4; $\frac{z}{h} = 0.354$.

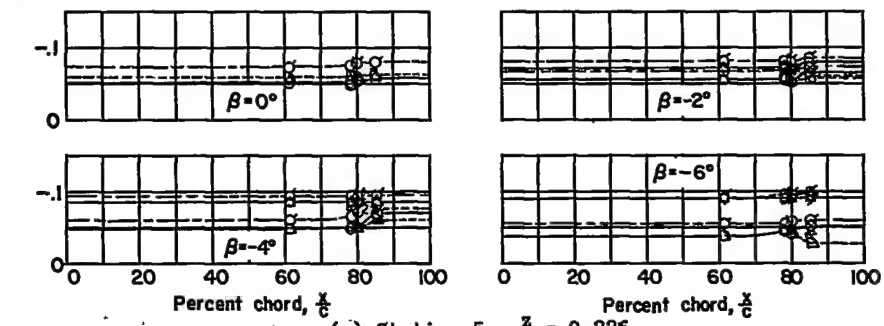

(e) Station 5: $\frac{z}{h} = 0.226$.

Figure 4.- Concluded.

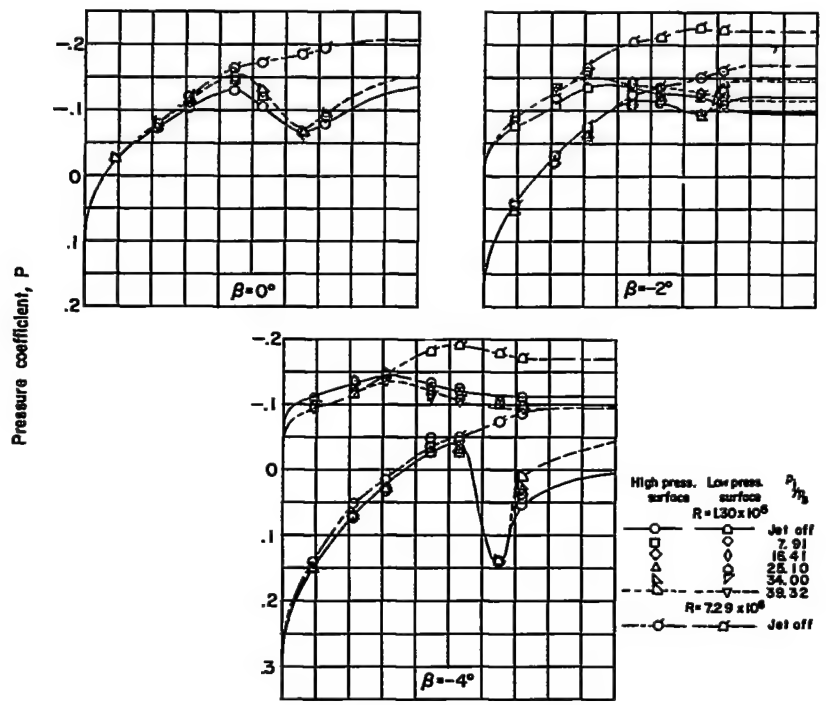

(a) Station 1; $\frac{z}{h}$ = 0.807.

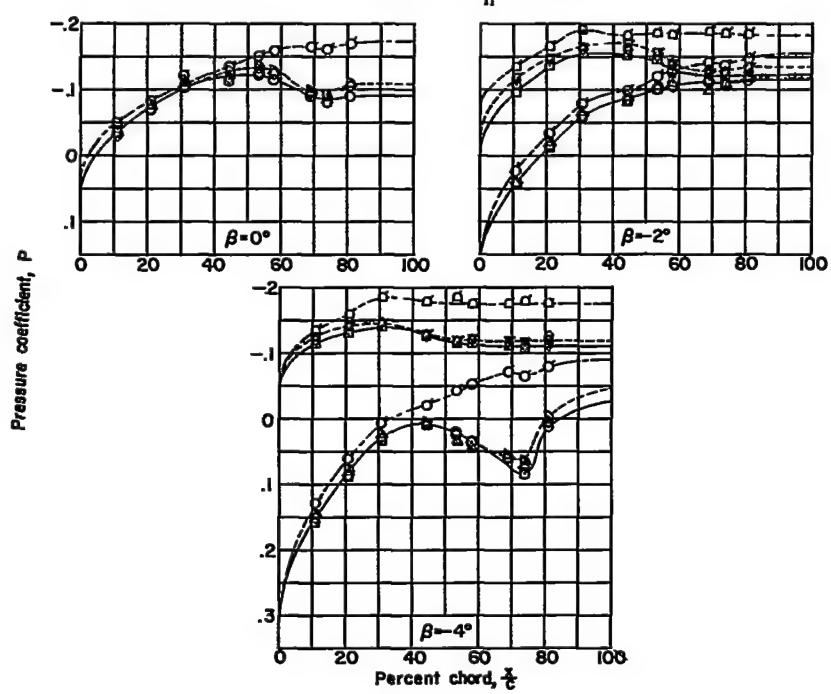

(b) Station 2; $\frac{z}{h}$ = 0.643.

Figure 5.- Effect of varying sideslip angle and jet pressure ratio on the pressure distribution over the vertical stabilizer and rudder at M = 1.93. $\alpha = 0^{\circ}$; $\delta_r = 0^{\circ}$.

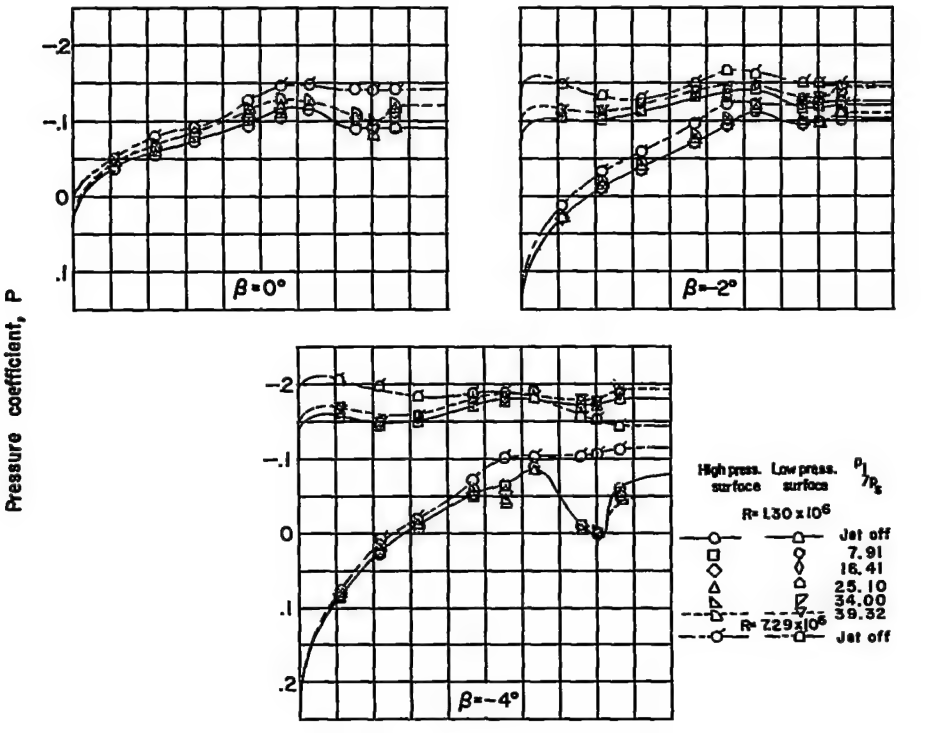

(c) Station 3; $\frac{z}{h}$ = 0.487.

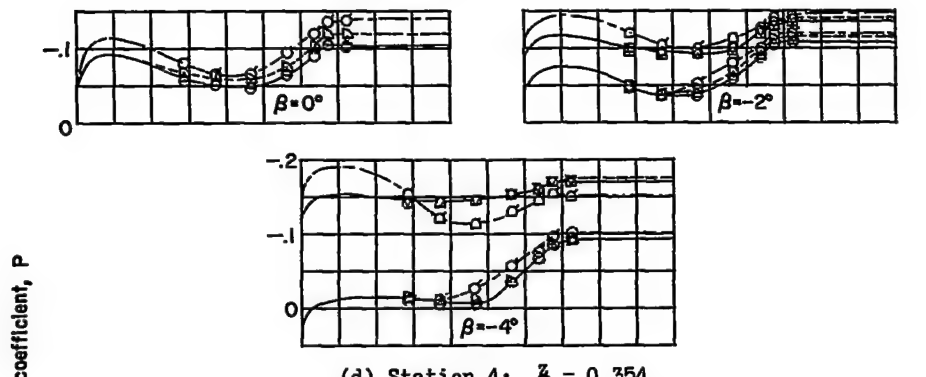

(d) Station 4; $\frac{z}{h}$ = 0.354.

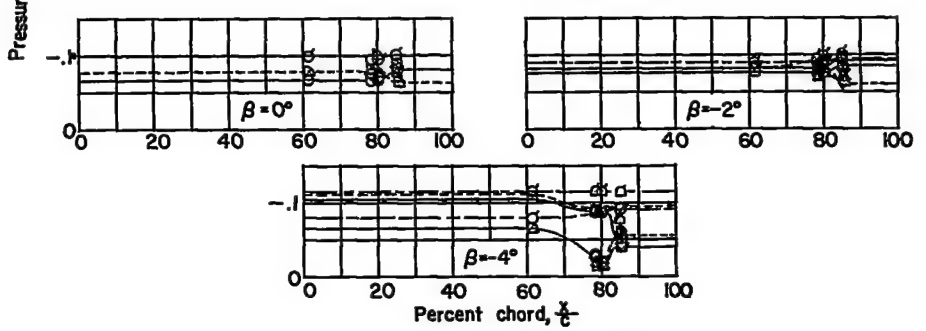

(e) Station 5; $\frac{z}{h}$ = 0.226.

Figure 5.- Concluded.

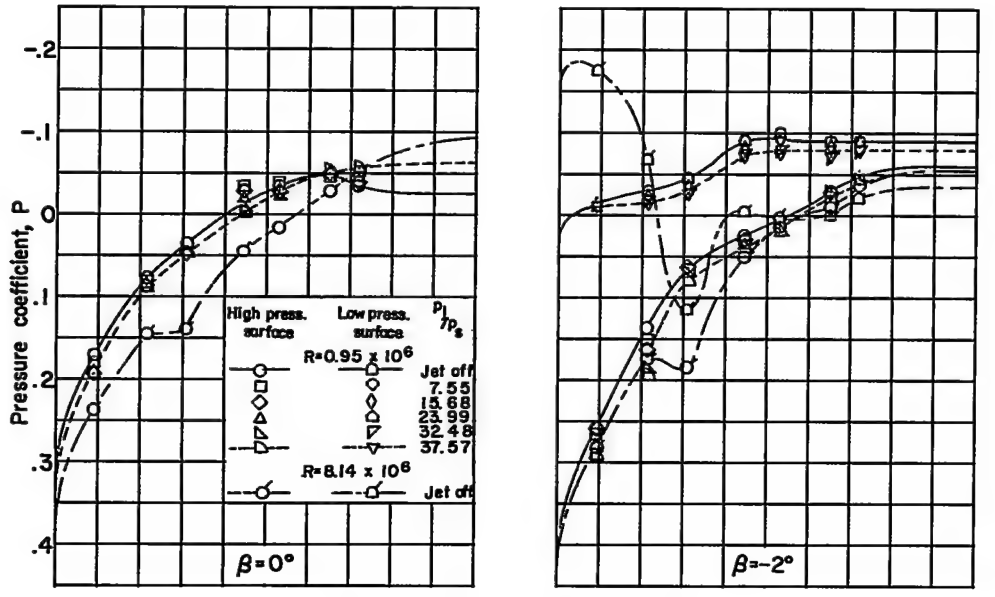

(a) Station 1; $\frac{z}{h} = 0.807$.

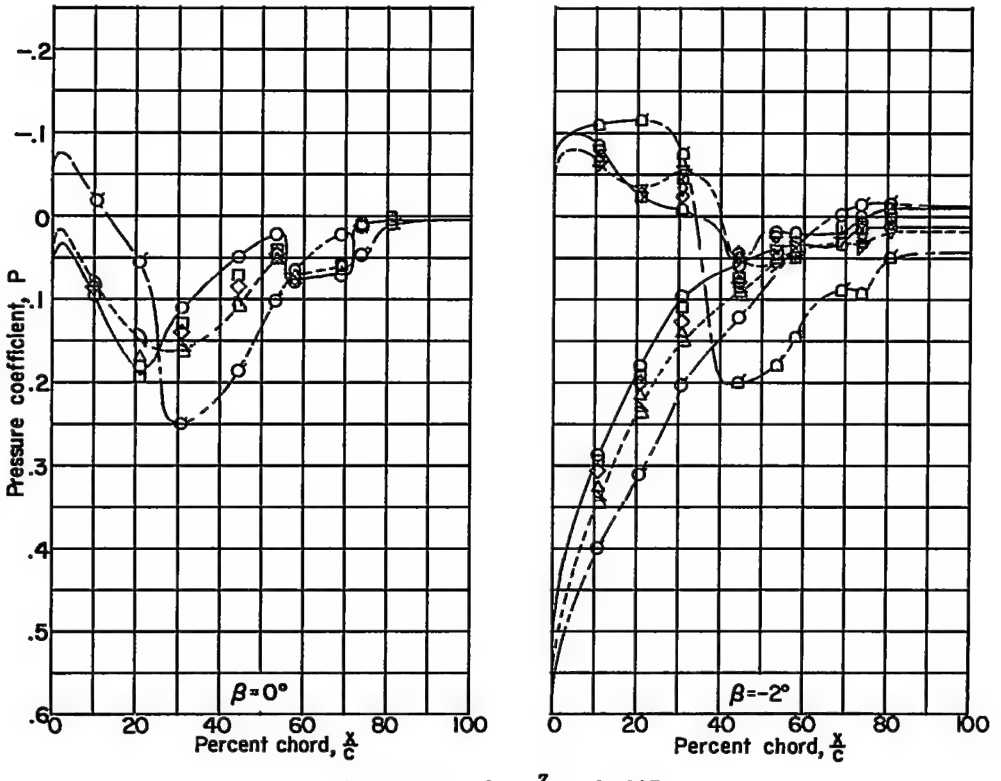

(b) Station 2; $\frac{z}{h} = 0.643$.

Figure 6.- Effect of varying sideslip angle and jet pressure ratio on the pressure distribution over the vertical stabilizer and rudder at $M = 1.62$. $\alpha = 0^{\circ}$; $\delta_r = 0^{\circ}$.

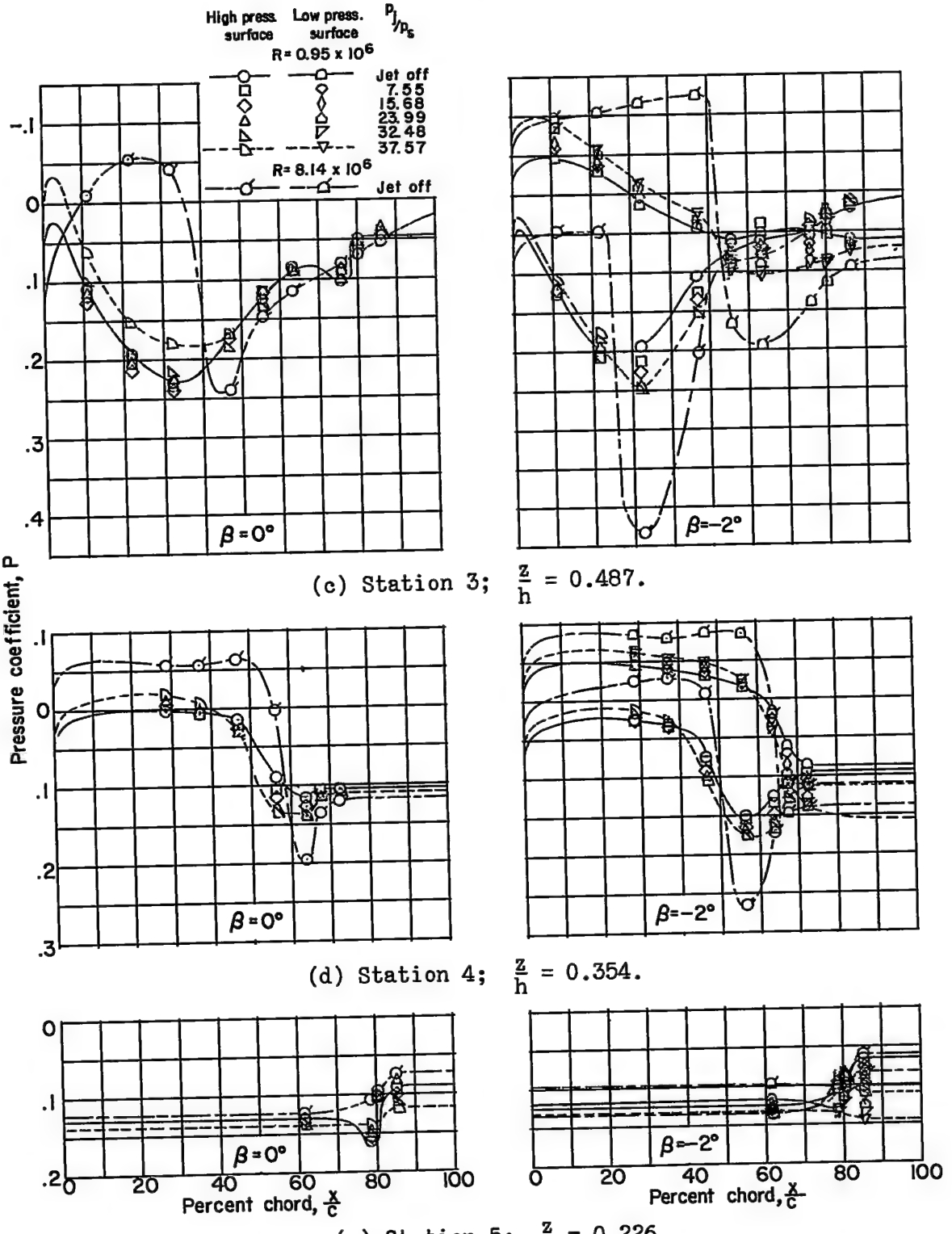

(c) Station 3; $\frac{z}{h} = 0.487$.

(d) Station 4; $\frac{z}{h} = 0.354$.

(e) Station 5; $\frac{z}{h} = 0.226$.

Figure 6.- Concluded.

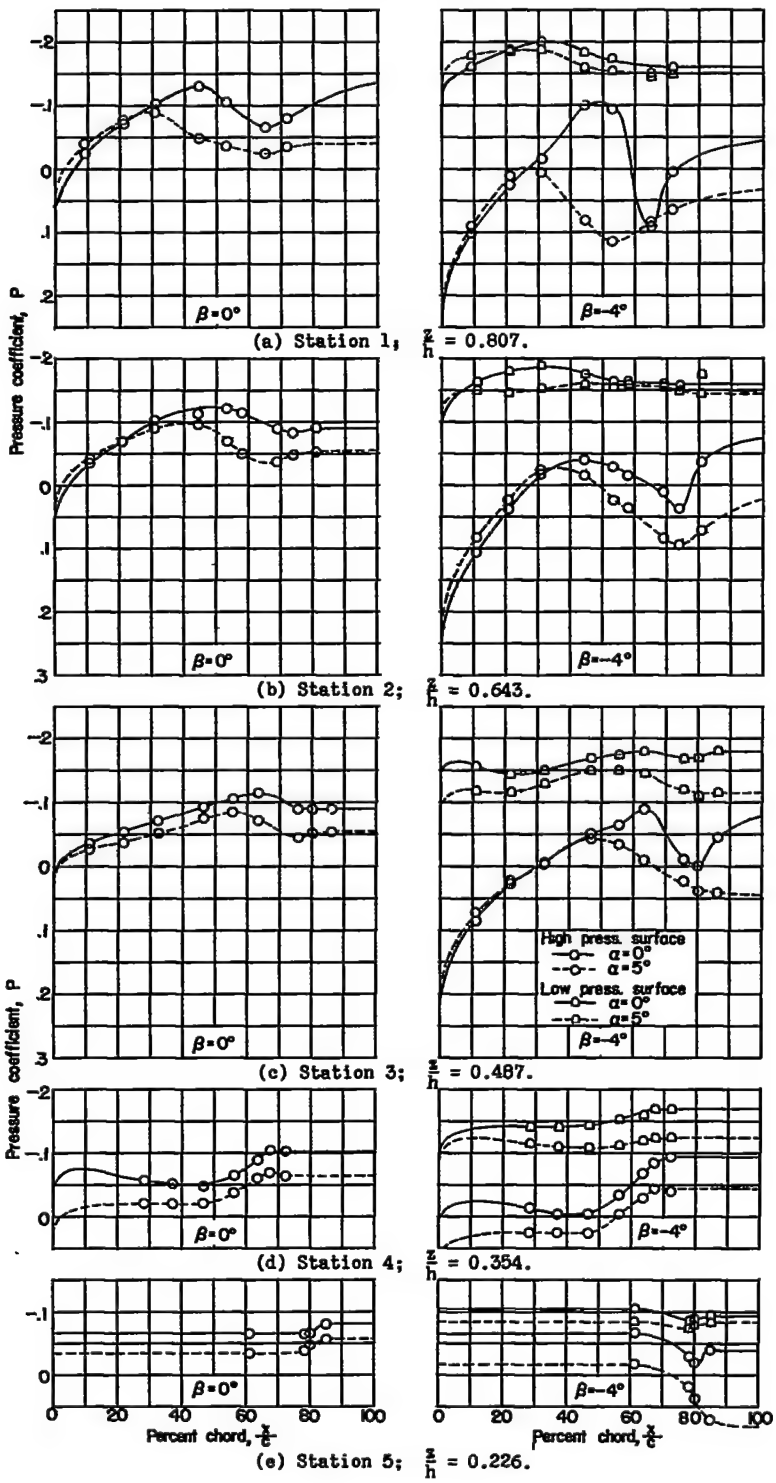

Figure 7.- Effect of varying angle of attack on the pressure distribution over the vertical stabilizer and rudder. M = 1.93; R = 1.30×10^6; jet off; $\delta_r = 0^\circ$.

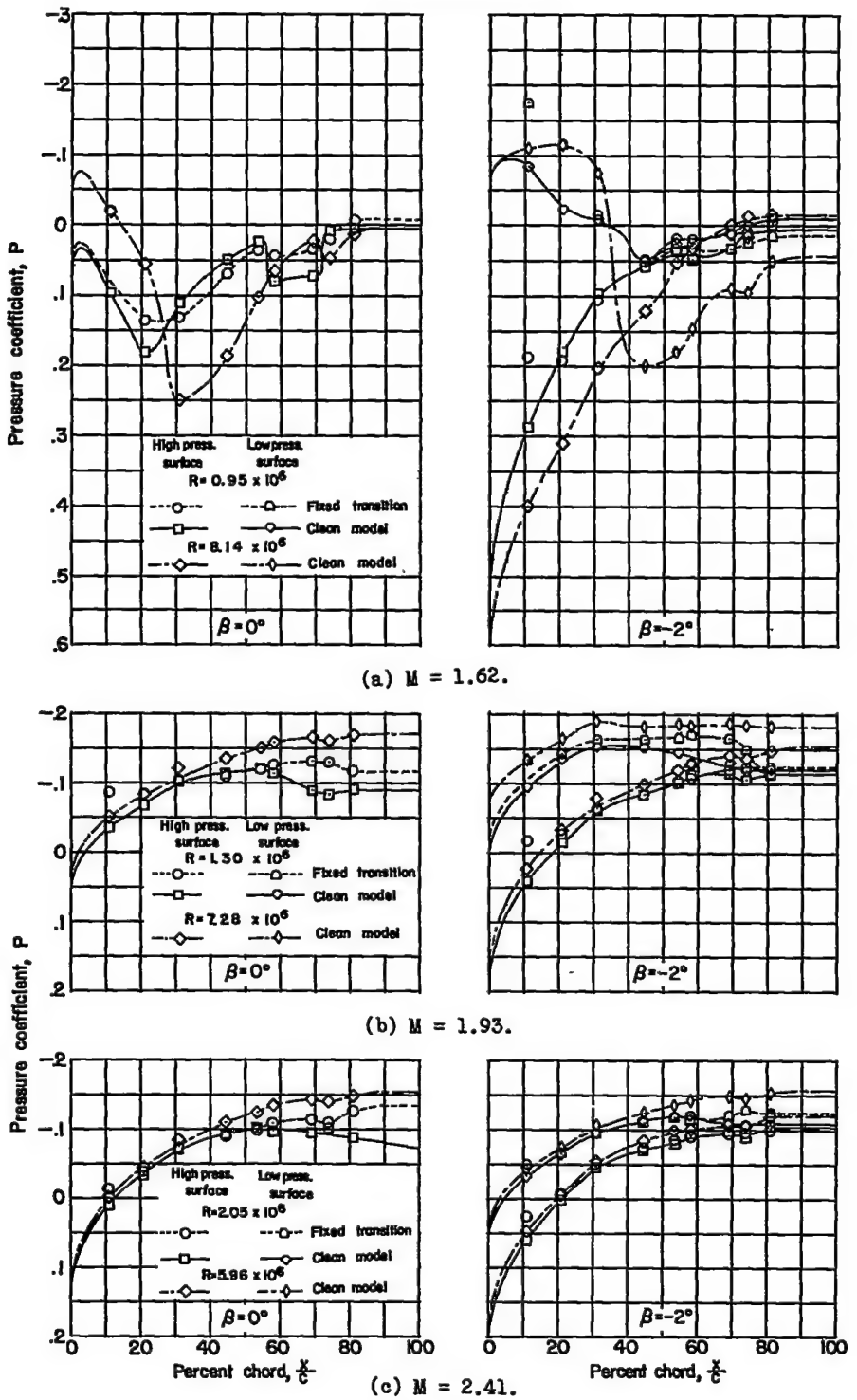

Figure 8.- Effect of fixing transition on the pressure distribution over the vertical stabilizer and rudder. Station 2, $\frac{z}{h}$ = 0.643; jet off; $\alpha = 0^{\circ}$; $\delta_r = 0^{\circ}$.

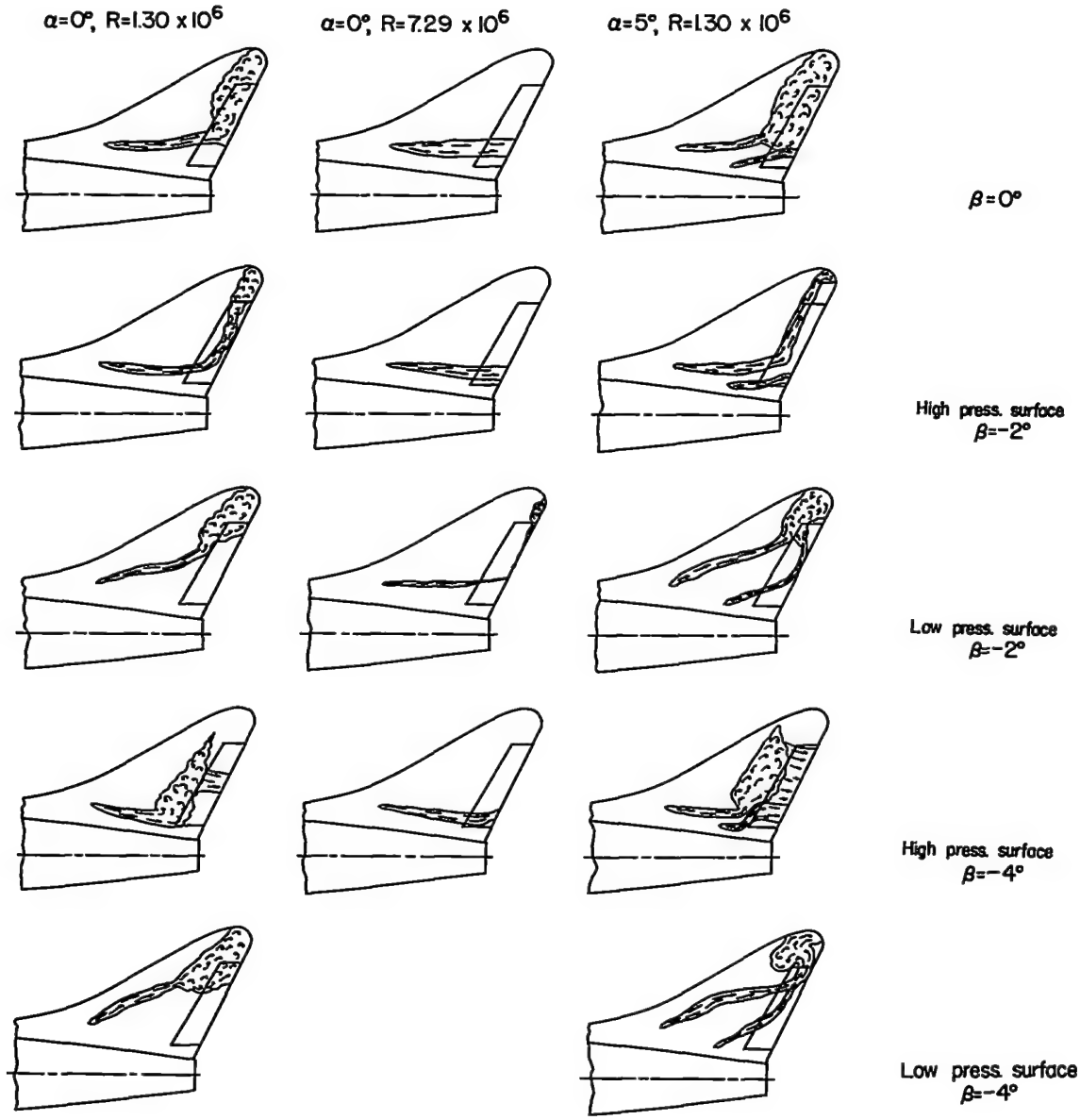

(a) M = 1.93.

Figure 9.- Sketch of ink-flow pattern illustrating effects of varying Reynolds number on the flow over the vertical stabilizer and rudder. Jet off; $\delta_r = 0^o$.

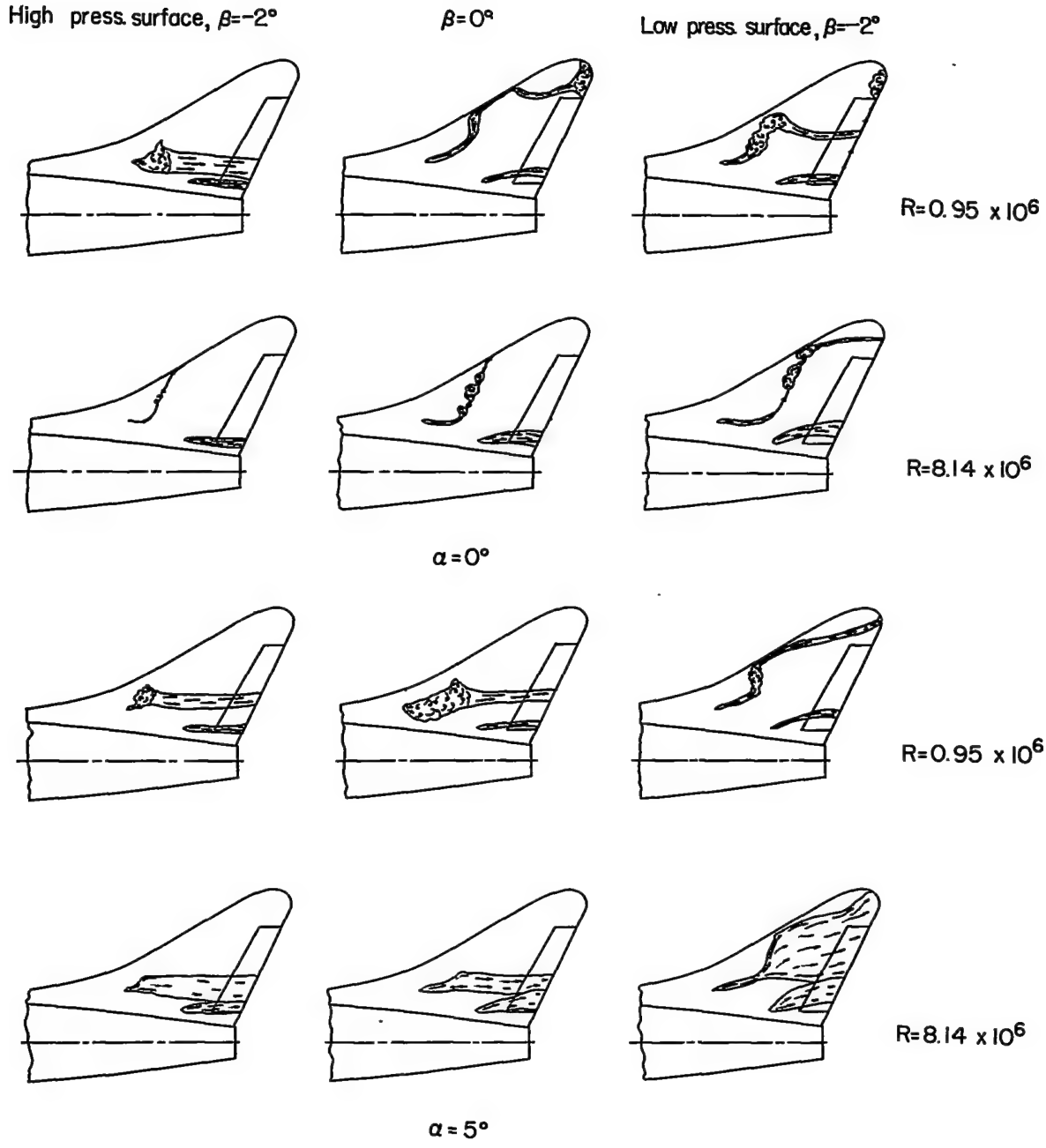

(b) M = 1.62.

Figure 9.- Concluded.

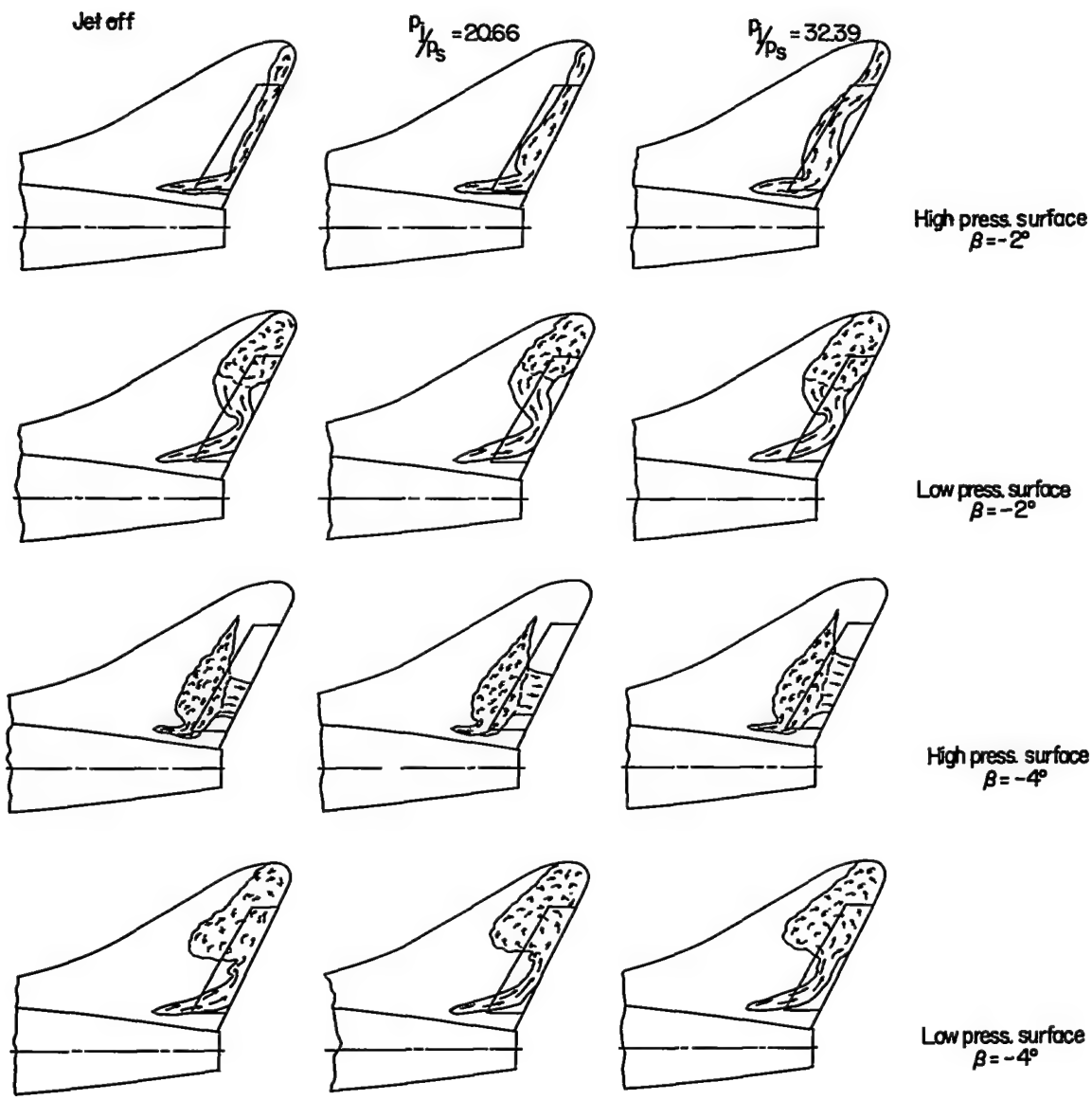

(a) $M = 1.93$; $R = 1.30 \times 10^6$; $\alpha = 0°$.

Figure 10.- Sketch of ink-flow patterns illustrating effects of varying jet pressure ratio on the flow over the vertical stabilizer and rudder. $\delta_r = 0°$.

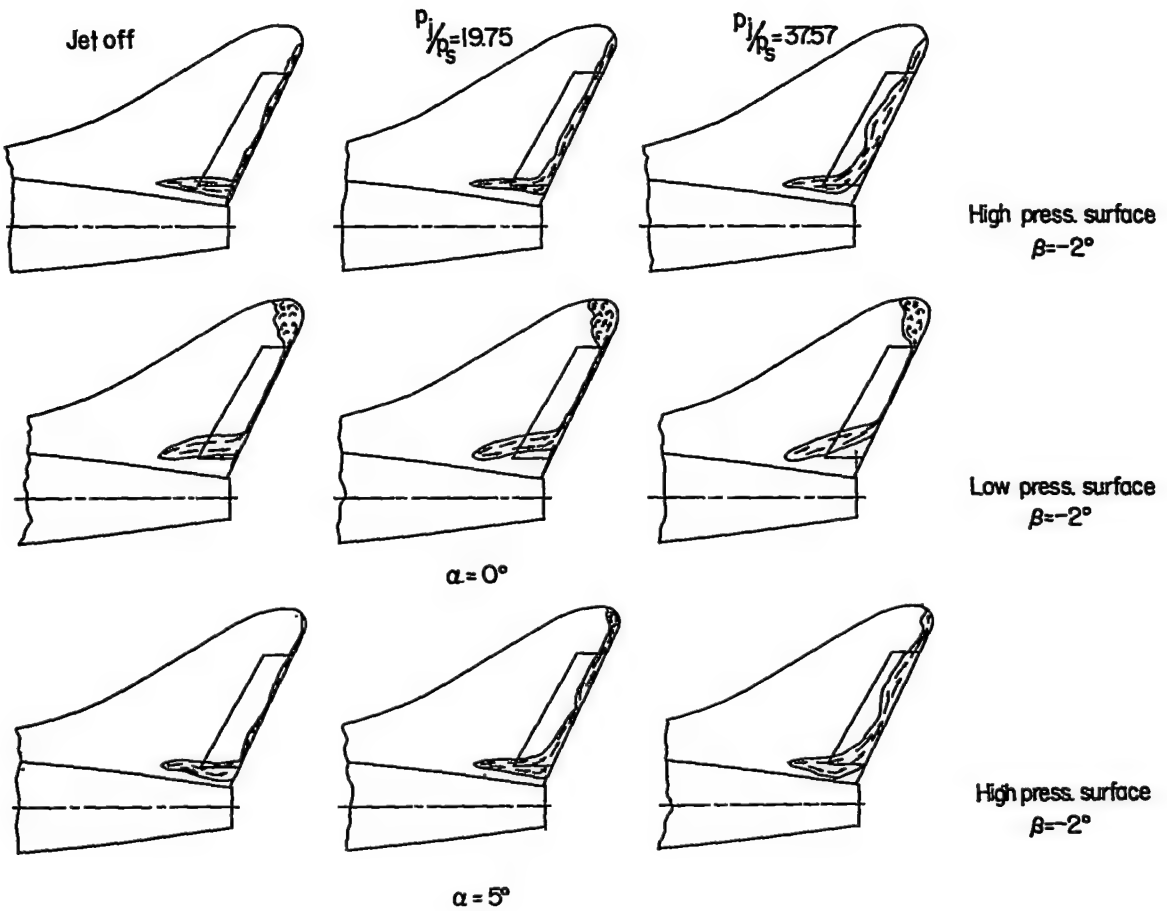

(b) M = 1.62; R = 0.95×10^6.

Figure 10.- Concluded.

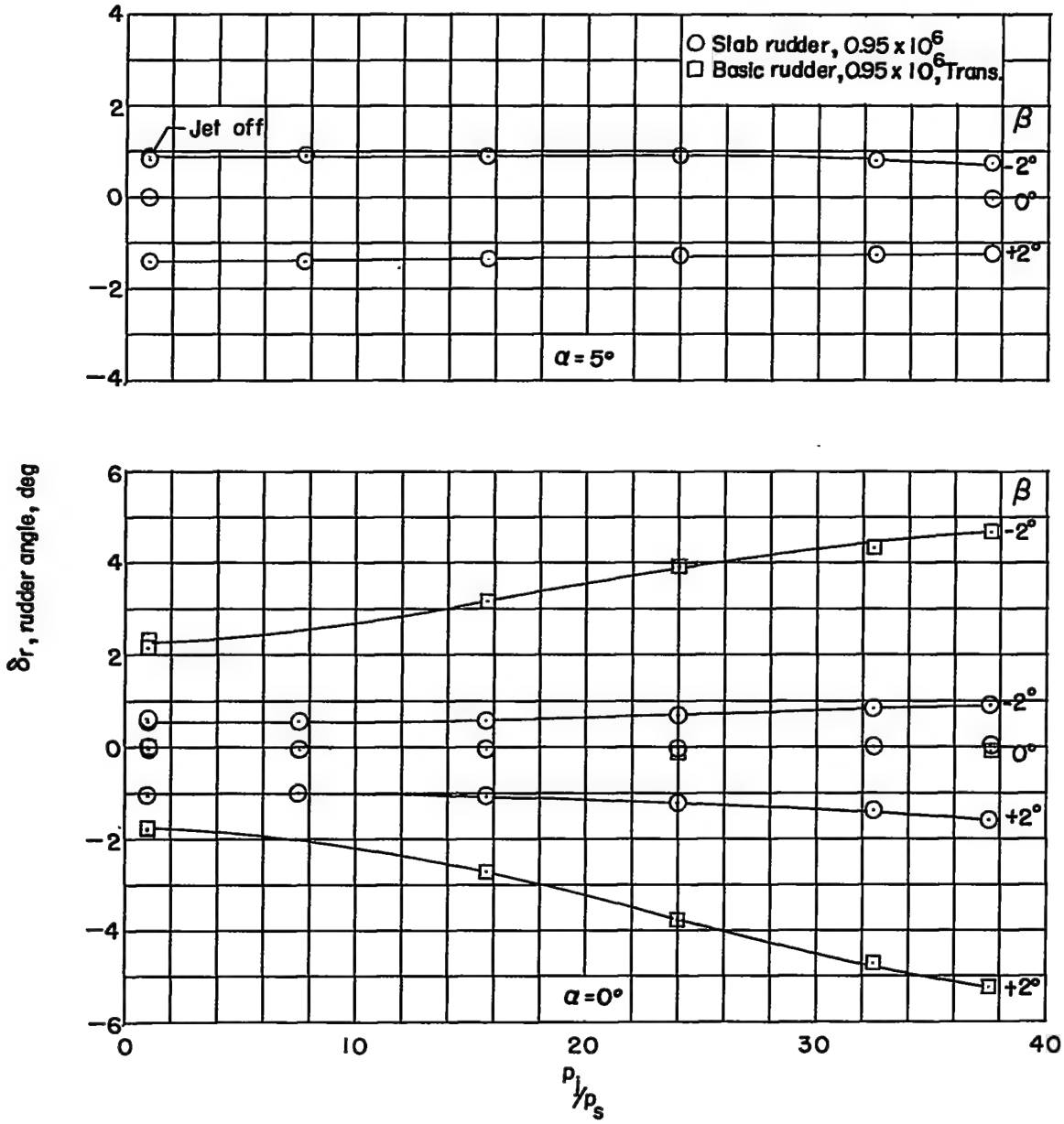

Figure 11.- Effect of varying jet pressure ratio upon the angle of the free-floating rudder. M = 1.62.

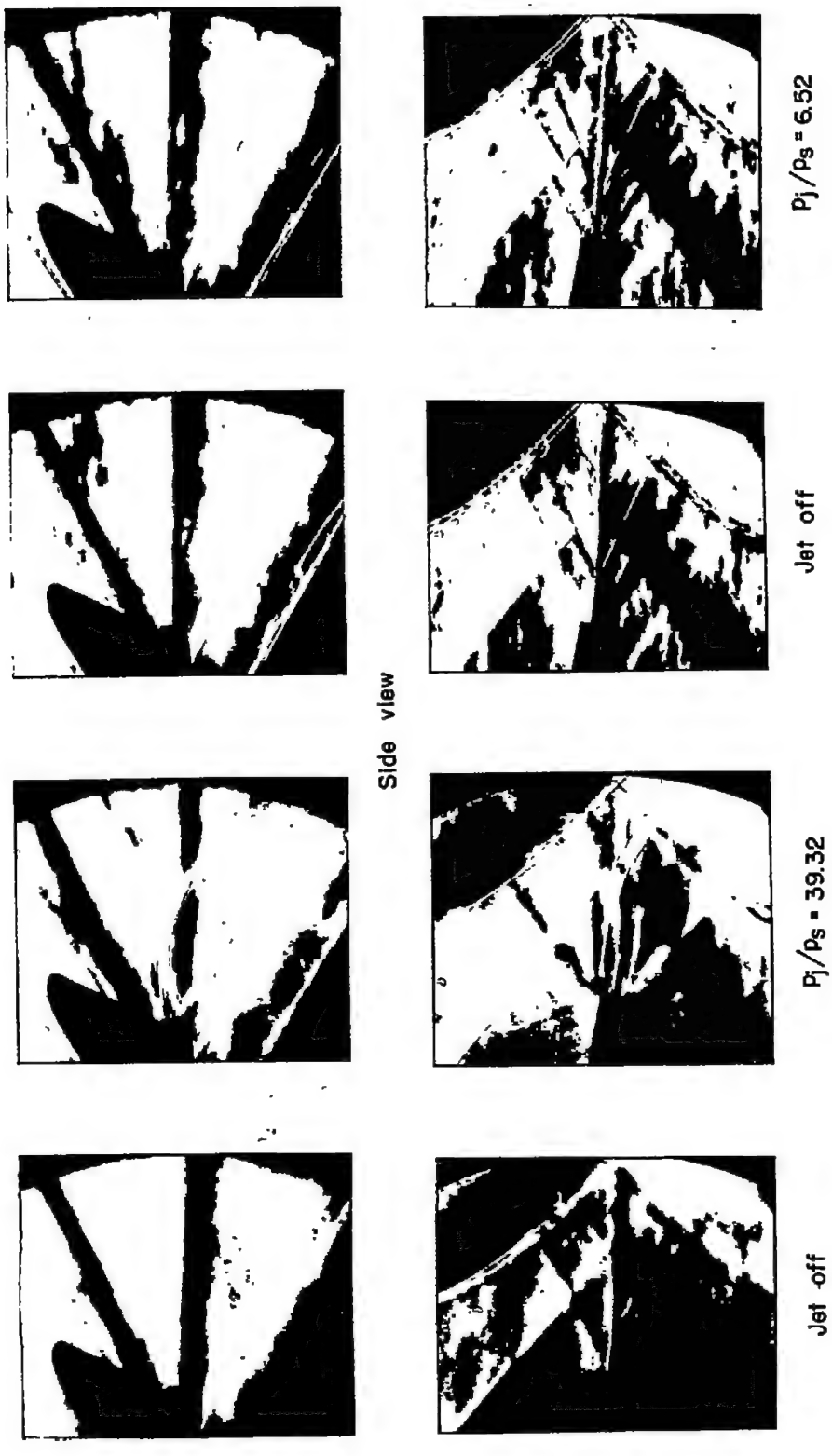

Figure 12.- Typical schlieren photographs illustrating the effect of jet pressure ratio upon the flow characteristics over the rear of the model and vertical stabilizer and rudder. $\alpha = 0^\circ$; $\beta = 2^\circ$; M = 1.93.

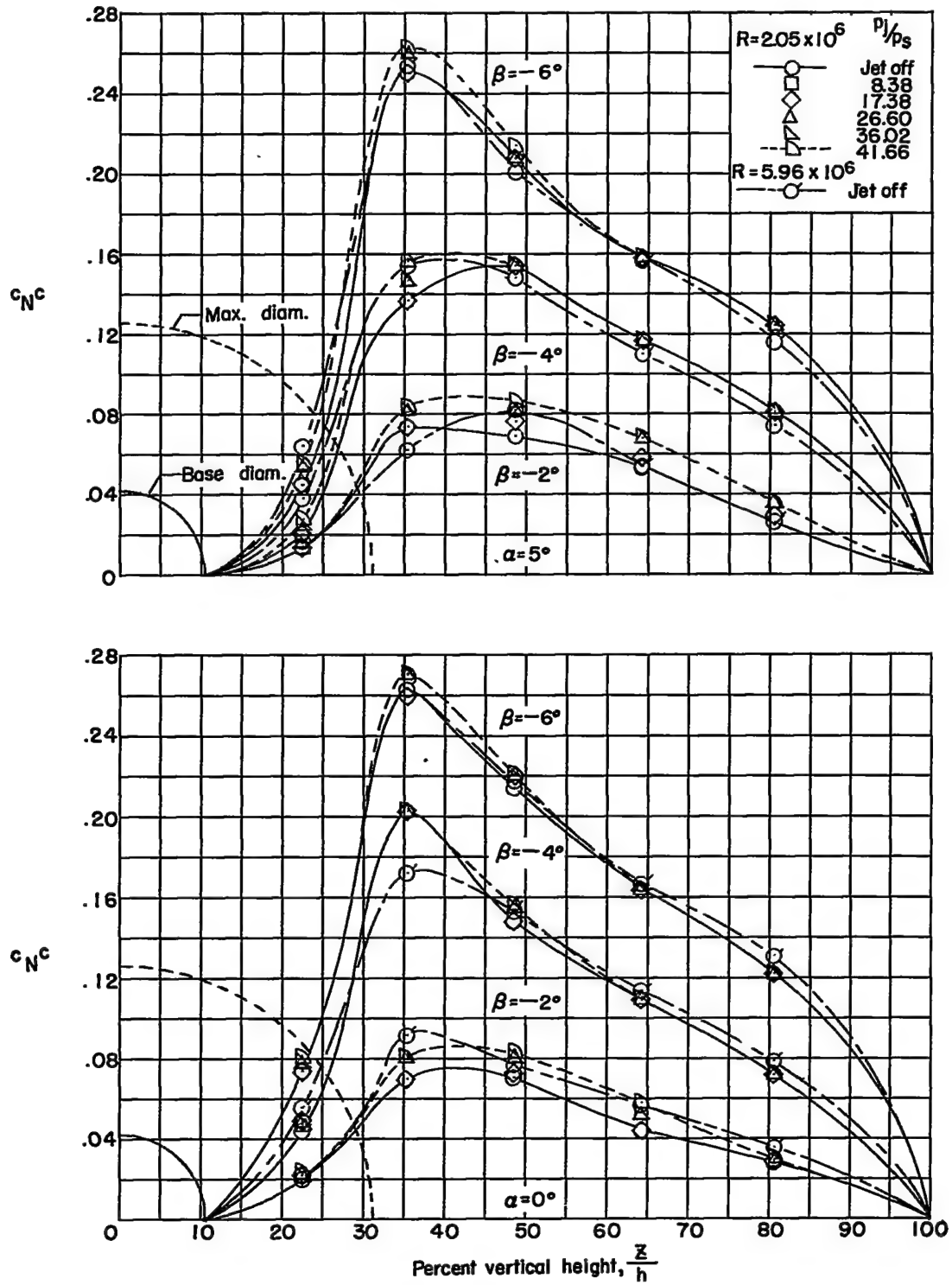

(a) M = 2.41.

Figure 13.- Spanwise variation of section loading coefficient.

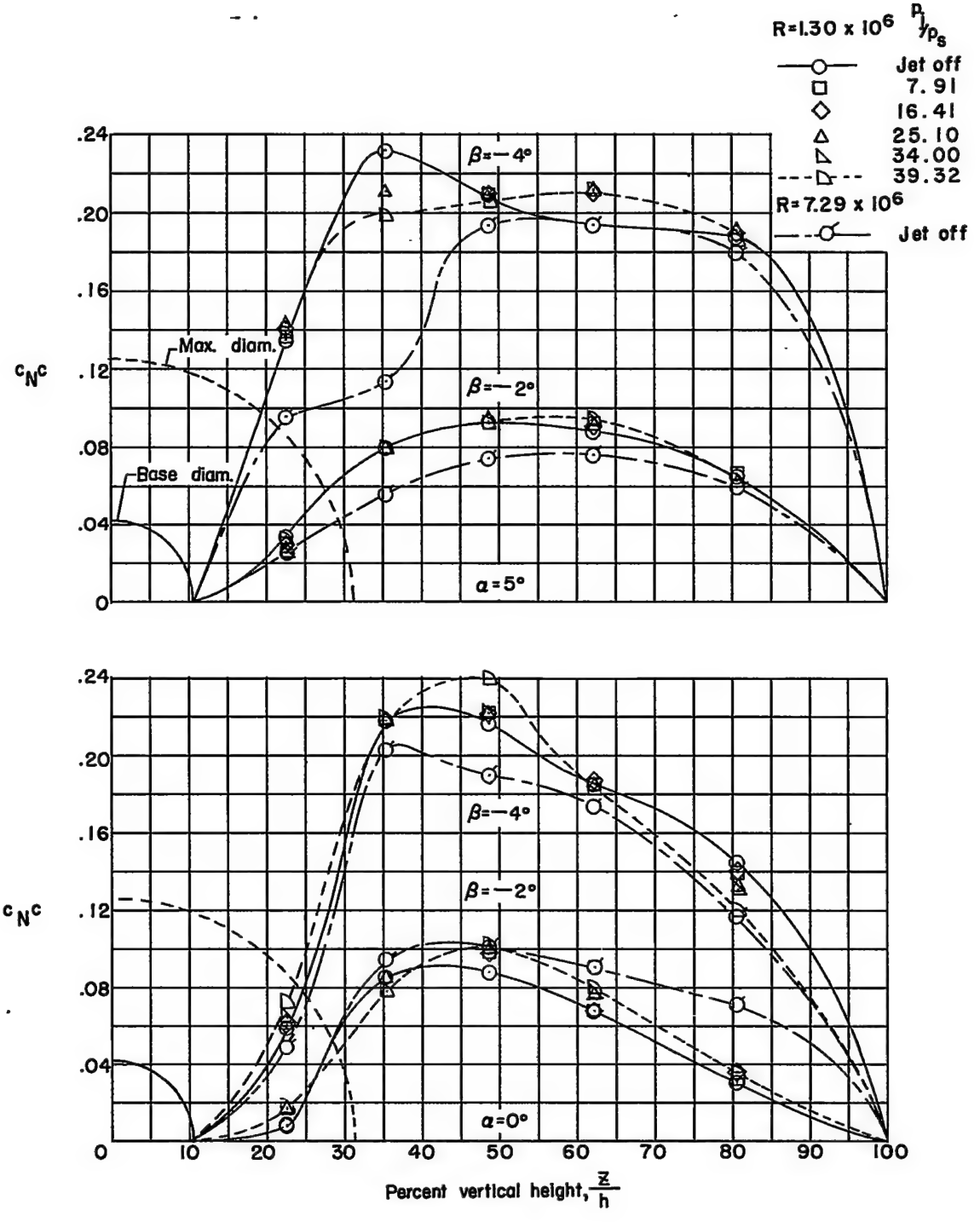

(b) M = 1.93.

Figure 13.- Continued.

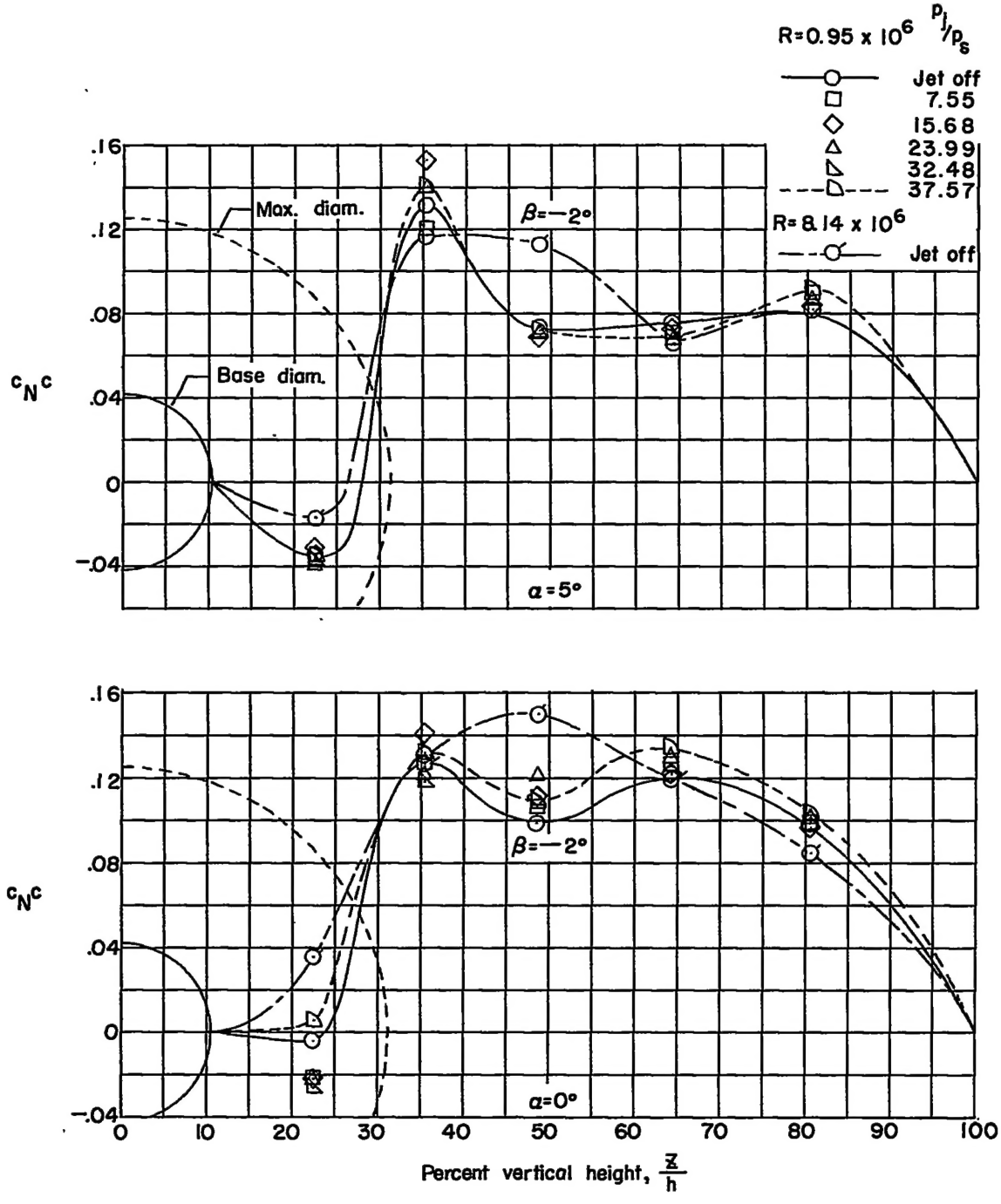

(c) M = 1.62.

Figure 13.- Concluded.

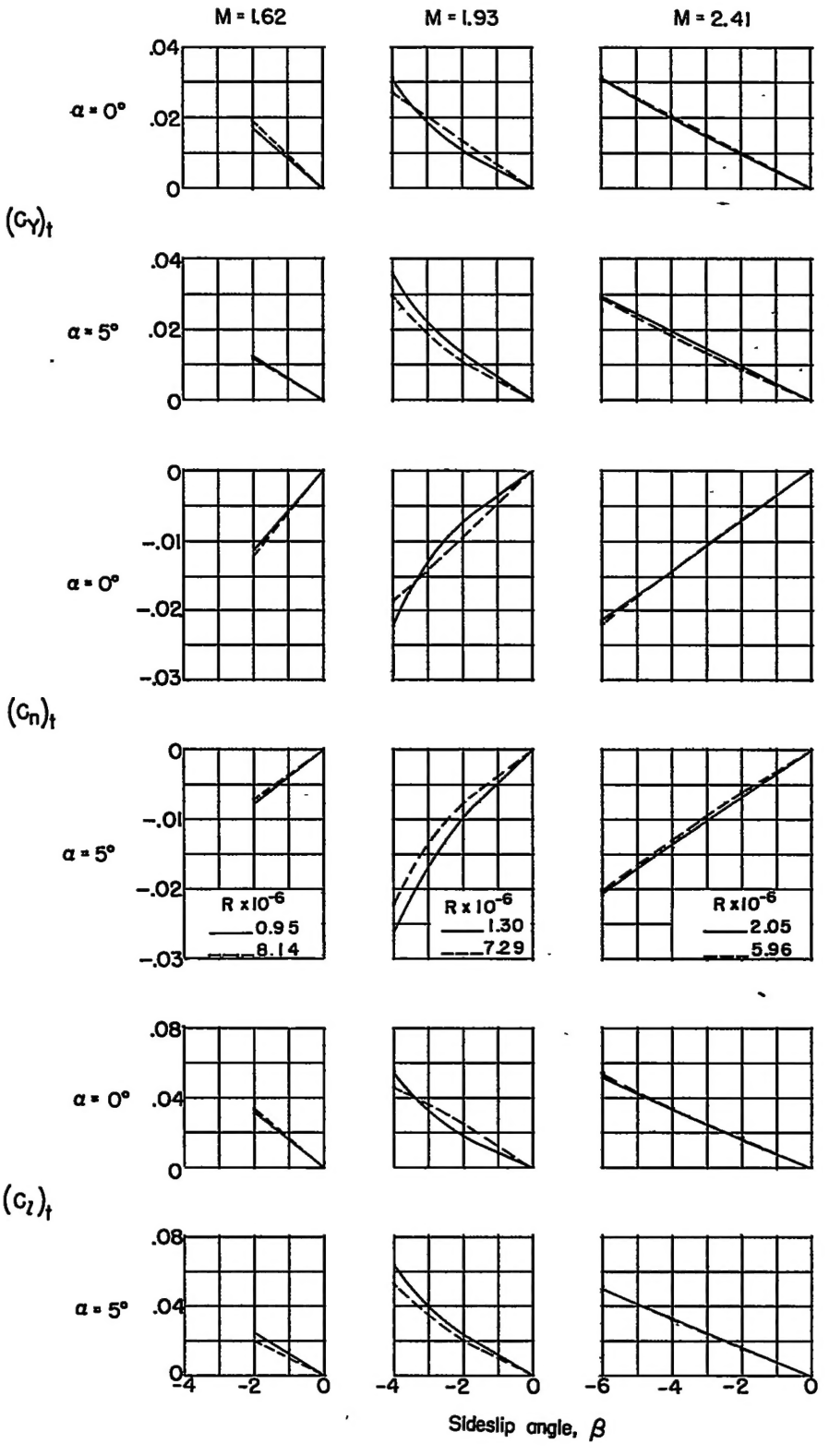

Figure 14.- Variation of sideslip force coefficients for the vertical tail with sideslip angle.

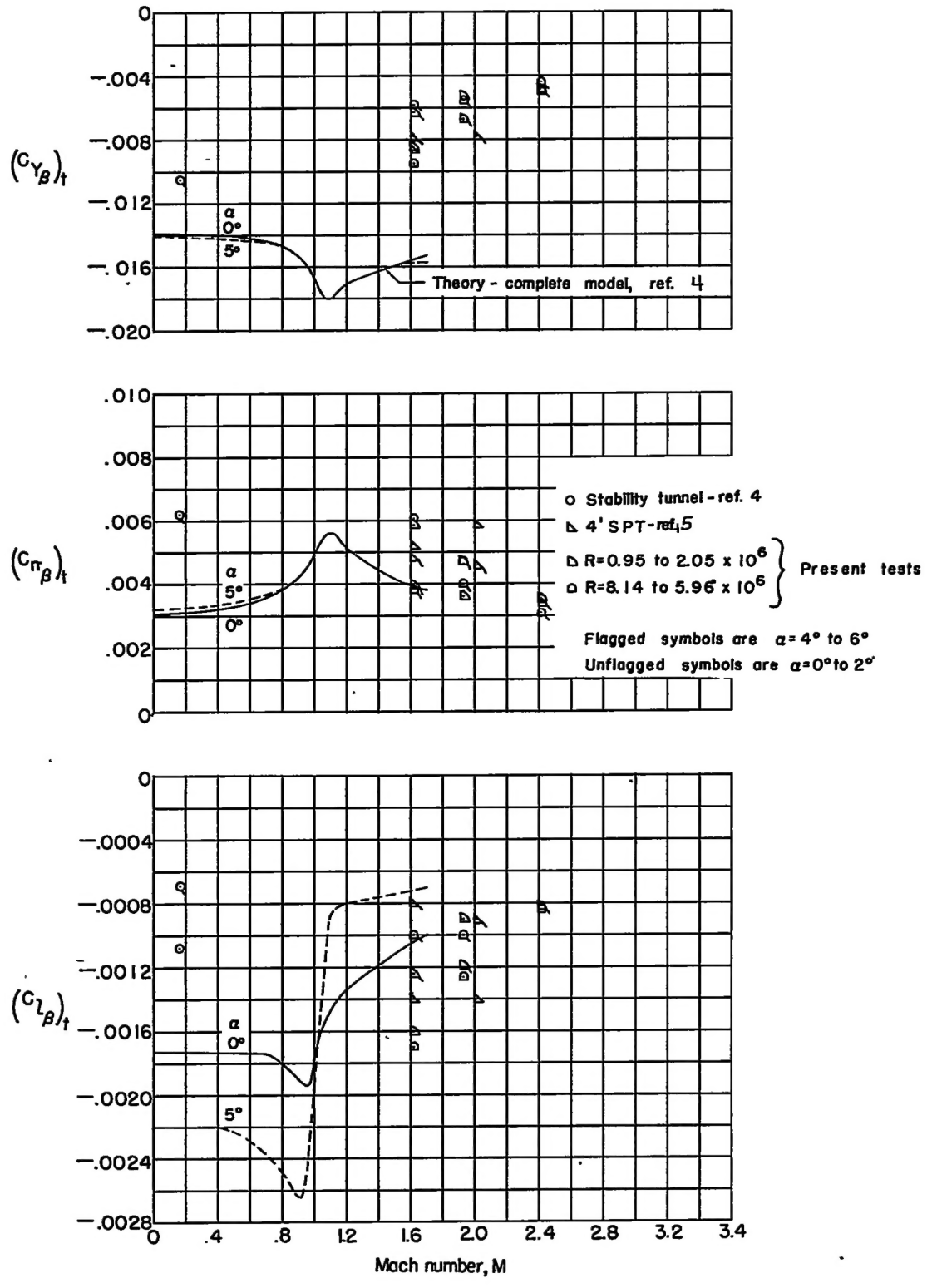

Figure 15.- Variation of sideslip derivatives for the vertical tail with Mach number. (Compilation of available wind-tunnel results.)

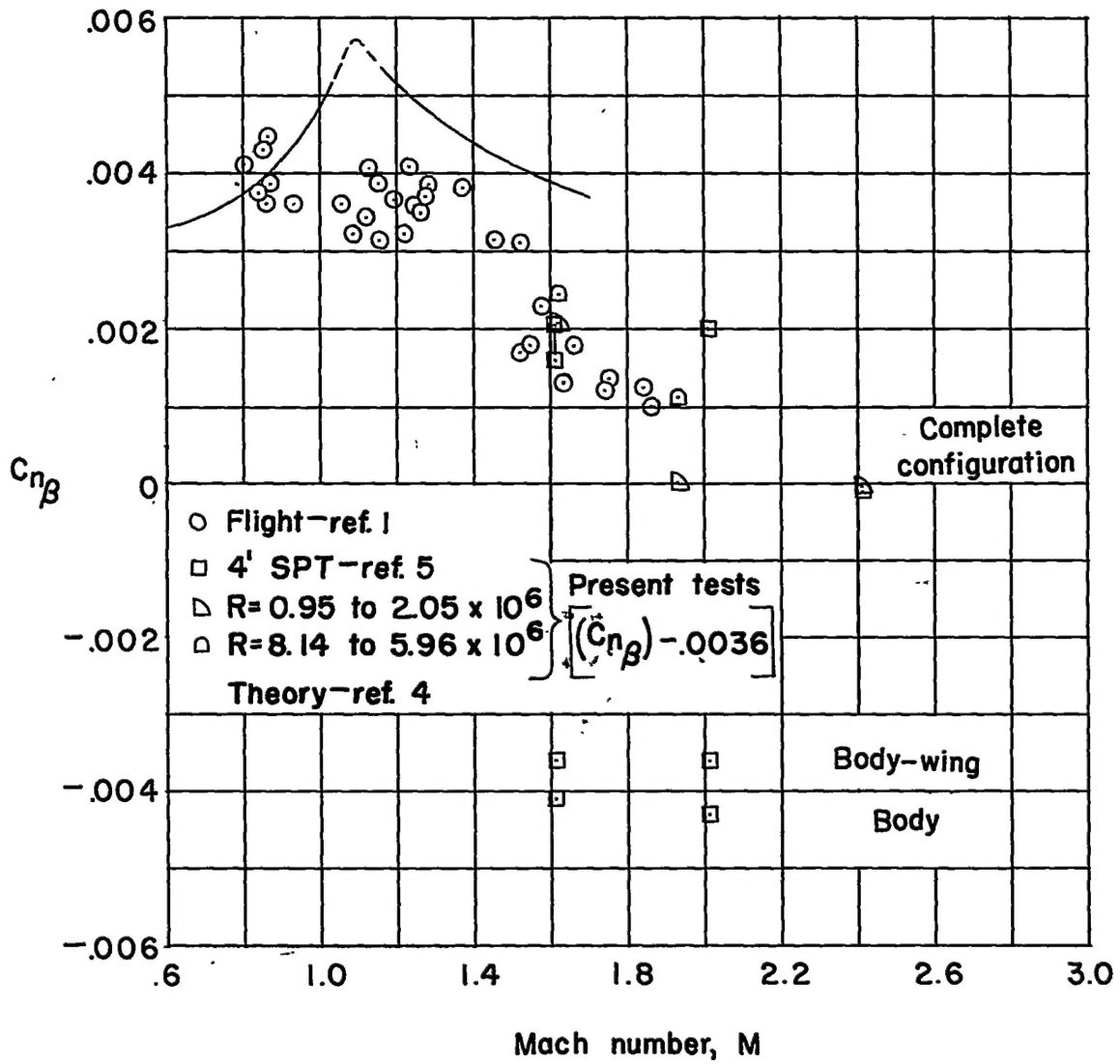

Figure 16.- Variation of the static-directional-stability derivative with Mach number.

[redacted]